POLITECNICO DI TORINO

MASTER's Degree in Biomedical Engineering

MASTER's Degree Thesis

Automatic classification of fragile subjects using sEMG signals recorded with REMO®.

Supervisors

Prof. Gabriella OLMO

Prof. Paolo ARIANO

Candidate

Sarah SACCO

Academic Year 2023/2024

Abstract

The concept of fragility has proven to be a challenging one to define with precision. One of the most significant challenges in this regard is the lack of consensus concerning the precise nature of the phenomenon.
Frailty is one of the leading causes of morbidity and premature mortality in older people. An international standard definition has yet to be established. A number of different measurement methods have been developed, including: The Fried frailty phenotype, the Tilburg Frailty Indicator (TFI) and the Frailty Index.
The objective of this study is to analyse muscle activity in order to determine whether it is possible to detect frail subjects by means of simple forearm exercises. Indeed, surface electromyography (sEMG) may be employed as an additional method for evaluating frailty, as one of the defining characteristics of frailty is a reduced ability to perform exercise and motor activity. In particular, eight-channel surface electromyography was extracted from the forearm of elderly subjects using the wearable armband Recognition Movement (REMO®), developed by Morecognition s.r.l. The subjects were previously classified into two categories (frail/not frail) using the Fried frailty phenotype and Tilburg Frailty Indicator. The objective is to develop an automatic classifier to demonstrate the feasibility of identifying frailty through the use of sEMG, with a view to establishing an automatic measurement technique.

A me
a te,
Nonna G.

Table of Contents

List of Tables

List of Figures

Acronyms

TFI
Tilburg Frailty Indicator

EMG
Electromyography

s-EMG
Surface electromyography

MU
Motor Unit

AP
Action Potential

PASE
Physical Activity Scale for the Elderly

CES-D Scale
Center for Epidemiologic Studies Depression Scale

PSD
Power Spectral Density

RMS
Root Mean Square

SNR
Signal to Noise Ratio

std
Standard Deviation

MVC
Maximum Voluntary Contraction

IIR

Infinite impulse response filter

VAR

Variance

STD

Standard deviation

MAV

Mean Absolute Value

WL

Waveform Length

WAMP

Willison Amplitude

IsEMG

Integrated s-EMG

SSI

Simple Square Integral

ACT

Activation

f-MEAN

Mean Frequency

f-MEDIAN

Median Frequency

AR2

Second order autoregressive coefficient

AR6

Sixth order autoregressive coefficient

SSC

Slope Sign Changes

AAC

Average Amplitude Change

ENTR

Entropy

CREST

Crest Factor

KURT

Kurtosis

SKEW

Skewness

TRS

Training set

TS

Test set

PCA

Principal Component Analysis

SVM

Support Vector Machine

RBF

Radial Basis Function

TN

True Negative

TP

True Positive

FN

False Negative

FP

False Positive

Chapter 1

Introduction

The concept of frailty has proven to be a challenging one to define with precision. Moreover, there is no unambiguous and universally accepted method for defining the fragility of a subject.
The concept of frailty is not solely predicated on age as a differentiating factor. Accordingly, even an individual of a relatively young age can be considered frail. However, among the over-65s, fragility is often associated with a number of factors, including chronicity, comorbidity, functional impairment, polypharmacy and social and health problems. These factors play a decisive role in the association between frailty and old age.[1] It is of vital importance to learn to recognise a frail person, as frailty is known to be closely linked to a decrease in quality of life, an increased risk of falls, disability or comorbidity, and consequently an increased risk of mortality.[2][3] It is therefore of critical significance to identify frail elderly individuals at an early stage and implement appropriate interventions.[3]

The aim of this study was to identify a novel approach to the assessment of frailty from a physical perspective. A method that could be employed in conjunction with those currently in use and be carried out independently. The classifier was thus constructed to distinguish between frail and non-frail persons based on electromyographic signals acquired from a wearable device developed by Morecognition s.r.l..

1.1 Frailty measurements

The concept of frailty encompasses a multitude of domains, including physical, psychological, and social aspects. Professionals identify and address the various dimensions of the same condition, emphasising its multidimensional nature.[4]
Fried defines it as a physiological syndrome characterised by a reduction in functional reserves and decreased resistance to stressors, resulting from the cumulative decline of multiple physiological systems, which renders the individual vulnerable and susceptible to adverse consequences.[5] Furthermore, studies by Fried et al. have demonstrated that frailty and comorbidity are predictors for disability. It has been observed that the latter leads to a worsening of the former, and that having a comorbidity may contribute to the onset of frailty. This analysis has led to the formulation of a phenotype (a set of observable characteristics relating to a subject) of physical frailty. The following conditions were analysed:

- Unintentional weight loss;

- Fatigue;
- Reduced muscle strength;
- Reduced physical activity;
- Reduced walking speed.

A score between 0 and 5 is assigned to each item. A subject is defined as frail when three or more of the listed criteria are met, pre-frail when one or two are met, and otherwise non-frail.[5] This approach avoids the need for a prior clinical assessment, allowing it to be applied at the subject's first contact. The Fried phenotype is firmly based on the theory of biological causes and, through numerous epidemiological studies, has been demonstrated to be effective in detecting an increased risk of adverse clinical events, including mortality. However, this methodology has certain limitations. For instance, it exclusively assesses physical factors, some of which are not commonly used in clinical settings (such as grip strength). Furthermore, it lacks an analysis of psychosocial factors related to frailty.[6]

Another analysis defines frailty as a disorganisation of physiological systems that can be estimated through the examination of functional status, cognitive and physical deficits, psycho-social risk factors and geriatric syndromes. This allows for the reconstruction of a comprehensive picture of potential adverse risks.[7] This perspective acknowledges a multiplicity of variables, extending beyond the biomedical domain to cognitive and psycho-social conditions, as well as geriatric considerations.[8] In light of this latter definition, the Frailty Index was devised as a means of measuring accumulation of deficits.[9] Such deficits include, but are not limited to, reduced daily activities, reduced physical and cognitive performance, depression, disability, or any other illness. Each of these deficits is associated with a value between 0 (indicating no deficit) and 1 (indicating the presence of a deficit). Intermediate values are also permitted to capture the various degrees of the condition.

Further and subsequent analysis led to the development of an additional concept of frailty. This formula was introduced by Gobbens and colleagues, who conducted a comprehensive study of the existing literature on the concept of frailty by consulting various experts. These experts were drawn from a range of fields, including geriatric medicine, gerontology, nursing, (bio)statistics, psychology, general practice, healthcare, and social inclusion. This model conceptualises frailty as "a dynamic state" in which an individual experiences a decrement in one or more areas of human functioning (physical, psychological, and social) due to the influence of various factors, thereby increasing the risk of adverse outcomes.[10] In accordance with this line of reasoning, an additional frailty analysis tool was developed (the Tilburg Frailty Indicator), which differs from its predecessors in that it is completely self-diagnostic and does not present questions about disability. This decision was, in fact, influenced by numerous studies that have highlighted the distinction between disability and frailty. The latter is perceived as a state of pre-disability, whereas the former is regarded as a distinct entity.[11][12]
The Tilburg Frailty Indicator (TFI) is a questionnaire comprising multiple sections, which are to be answered independently by the subject. The instrument is divided into two sections. Section A comprises ten questions dealing with the determinants of frailty, including gender, age, place of birth, education, and occupation. Section B contains 15 questions on the components of fragility, which are divided into three categories: physical components, psychological components, and social components. The physical components include involuntary weight loss, physical activity, and lack of balance. The psychological

components include memory loss, anxiety, and nervousness. The social components include whether the subject lives alone and whether they miss other people. The initial section presents a series of questions with multiple-choice or open-ended responses. The subsequent section comprises dichotomous questions (*yes/no*), whereas some questions allow for three possible answers, which are provided for respondents' convenience. The response options were *yes, sometimes* and *no*. Subsequently, each question is evaluated according to the answer provided and a score of 0 or 1 is assigned. This allows the TFI score to be calculated. A total score of five or more is indicative of a person who may be classified as frail.[3][13][14]
Previous findings have validated the TFI as a tool for frailty and its domains (Gobbens, van Assen *et al.*, 2010b), demonstrating the expected correlations between frailty as measured by the TFI and related frailty measures. As a multidimensional assessment of frailty, the TFI is a valuable tool for predicting disability, various indicators of healthcare utilisation and quality of life of older people at one and two-year intervals. It can be employed as a preliminary screening tool by community caregivers to identify individuals who may benefit from more detailed assessments and tailored interventions, with the aim of improving the quality of life of frail older persons.[15]

In the course of time, a number of experts came together in order to develop a widely recognised definition of frailty, taking into consideration the various definitions that had been found in the literature up to that time. From the observation of the various definitions that had been taken into account, it was possible to derive the two fundamental principles on which the concept of frailty is based. The first of these principles, as mentioned above, concerns 'multidimensionality', which conceives frailty as a combination of problems involving different functional domains. The second principle, concerning 'continuity', emphasises the nature of a degenerative and potentially reversible process of frailty, originating from the interaction between personal and environmental factors. Consequently, it is proposed that frailty should not be conceived as a binary phenomenon, but rather as a nuanced entity to be analysed in its various facets.[16]

1.2 Evidence of muscle physiology

An integral part of frailty is the reduced ability to perform exercises and motor activity. Consequently, the objective of this work was to analyse muscle activity in order to determine whether it was possible to detect frail subjects by means of simple forearm exercises.

1.2.1 The skeletal muscle

Skeletal muscles are voluntary, therefore belong to the class of striated muscles. They constitute the majority of the body's muscle mass and are responsible for maintaining posture, stability and are essential for the execution of movement in all its forms.
The skeletal muscle tissue is composed of fascicles, each of which is comprised of numerous muscle fibres arranged parallel to one another. Each muscle fibre is enclosed in a plasma membrane, called sarcolemma, which contains the cytoplasm, designated as sarcoplasm. The primary intracellular structure and contractile unit are the myofibrils, which are arranged in a longitudinal orientation along the sarcoplasm (Figure 1.1a). The myofibrils

are encased in a network of cylindrical membranes, the sarcoplasmic reticulum, which is capable of storing the calcium ions (Ca^{2+}) that are essential for the initiation of muscle contraction. The sarcoplasmic reticulum is comprised of two terminal cisternae, which are in turn surrounded by a network of tubules, called T-tubules. These tubules diffuse through the sarcoplasm and, when a nerve impulse arrives, facilitate depolarisation and the consequent muscle contraction.
The sarcoplasm of a striated muscle fibre contains a multitude of myofibrils, elongated cylindrical structures that extend the length of the fibre. These myofibrils, which consist of bundles of short myofilaments, undergo shortening during contraction due to changes in the position of the proteins that compose them. These include contractile proteins (myosin and actin), regulatory proteins (tropomyosin and troponin), and structural proteins (nebulin and titin).
Myofibrils are defined by a fundamental unit, the sarcomere, which represents the functional contractile unit of striated muscle tissue. The sarcomere is composed of thick filaments in the centre, which are primarily composed of myosin, and thin filaments at the poles, which are primarily composed of actin. The interaction between actin and myosin is carefully regulated during the process of muscle contraction by the proteins troponin and tropomyosin. The arrival of calcium in the sarcoplasm plays a pivotal role in this process. Calcium ions (Ca^{2+}) bind to troponin, resulting in a conformational change that regulates the position of tropomyosin. This alteration results in the exposure or occlusion of the binding site on actin, thereby initiating or terminating the process of muscle contraction.[17]

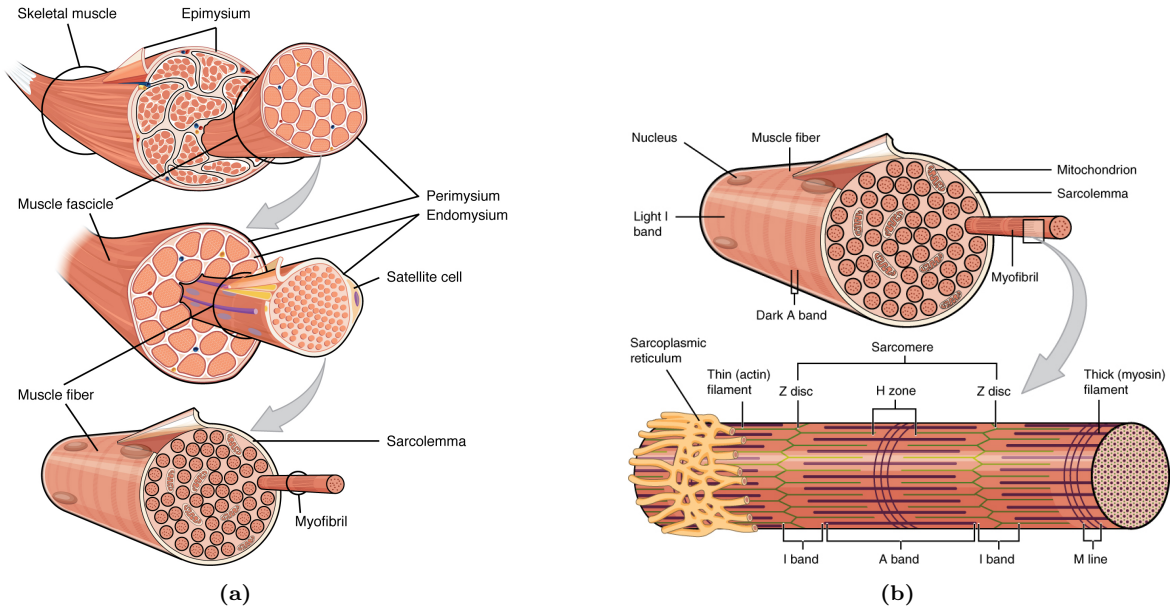

Figure 1.1: a) Skeletal muscle structure. b) Muscle fibre portion.[18]

In order to elucidate the mechanisms underlying muscle contraction and force generation, the sliding filament model is employed. This model posits that during the contraction of a muscle cell, the sarcomeres undergo shortening. This shortening is not due to the contraction of the filaments themselves, but rather to the sliding of the actin filaments along the myosin filaments, which reduces the overall length. The mechanism that leads to sliding is referred to as the crossbridge cycle. During this process, the crossbridges in the thick filaments alternately attach and detach from the thin filaments, pulling them towards the centre of the sarcomere. Although force is only produced during one phase of

the cycle, the muscle cell produces force continuously throughout the contraction, as the transverse bridges are out of phase with each other. As a result, when some bridges have started the cycle, others will have finished it, and so on. Upon cessation of the contraction, the thin filaments return to their original position passively.[17]

1.2.2 The contraction process and action potentials

Skeletal muscles are innervated by large nerve fibres, which originate from alpha motor neurons, located in the anterior horns of the spinal cord. Each nerve reaches the muscle via axonal extensions (nerve fibres), whose terminal branches each (synapses) make contact with a single muscle fibre. A motor unit (MU) is defined as the entirety of a nerve and all the muscle fibres it innervates. Consequently, each muscle fibre is typically innervated by a single nerve fibre, while each nerve innervates several muscle fibres, thereby constituting a motor unit. In the vicinity of the muscle fibre, the nerve endings diverge in numerous branches, which in turn terminate in dilatations. The collective term for these nerve endings and their branches is the motor plate. The site where the nerve endings and the muscle fibre meet is known as the neuromuscular junction.
The transmission of the nerve impulse occurs in a unidirectional manner, which allows for the distinction to be made between the pre-synaptic and post-synaptic components. The pre-synaptic component is characterised by the presence of numerous mitochondria and vesicles. Once a nerve impulse reaches the neuromuscular junction, the latter are released into the synaptic cleft, i.e. the area between the nerve and muscle membranes. The vesicles contain the skeletal muscle neurotransmitter acetylcholine (ACh), which binds to specific receptors located on the plasma membrane of the muscle cell (post-synaptic), inducing membrane depolarisation.
Prior to the arrival of a depolarising stimulus, namely when the muscle cell is in a resting state and is not contracted, it exhibits a low calcium concentration, which is a consequence of the activity of specific pumps that transport it from the cytoplasm to the reticulum. Furthermore, at this stage tropomyosin blocks the actin binding sites, preventing the cross-bridge cycle. The initiation of the cycle occurs following the binding of acetylcholine to receptors in the motor plate, which in turn induces membrane depolarisation, allowing sodium ions (Na^+) to enter via sodium channels. The influx of Na^+ alters the electrical charge within the muscle fibre, initiating an impulse that propagates to the surface of the sarcolemma and then penetrates the muscle fibre deeper into the T-tubules. Afterwards, the impulse activates so-called voltage-dependent receptors on the membrane of the tubules. These receptors undergo a conformational change, which in turn activates proteins on the membrane of the sarcoplasmic reticulum. Subsequently, the latter open and allow the passage of calcium ions (Ca^{2+}) from the reticulum to the cytoplasm of the muscle cell. The released Ca^{2+} ions then bind to troponin, which undergoes a conformational change and causes tropomyosin to move from its resting position, thus releasing the myosin binding sites and initiating the cross-bridge cycle.
The contraction terminates when the motor neuron ceases to transmit signals. This occurs as a result of a simultaneous closure of the proteins that allow the passage of calcium ions and a removal of the latter from the cytoplasm. The reduction in the concentration of calcium ions causes their dissociation from troponin, which returns to its initial resting state together with tropomyosin. This prevents the cross bridges from binding to actin. At this juncture, the elasticity of titin permits the thin filaments to revert to their original configuration.[17][19]

The process described above is underpinned by communication between neurons. This occurs via electrical signals, namely graded potentials and action potentials, which are changes in the membrane potential. These signals are generated when ion channels open or close in response to specific stimuli, altering the permeability of the membrane to certain ions.
Graded potentials represent small changes in the membrane potential, with the extent of these changes dependent on the intensity of the stimulus, hence the term 'graded'. The primary function of these cells is to generate an additional electrical signal, a significant modification of the membrane potential that propagates without attenuation, the action potential (AP). In order for the latter to be triggered, a number of graded potentials must collectively exceed a specific threshold value. In the absence of graded potentials, the resting membrane potential of the neuron is -70mV. This is maintained by the sodium-potassium pump, which regulates the concentrations of sodium and potassium ions inside and outside the membrane. Upon the emergence of one or more excitatory graded potentials within the neuron, the membrane potential reaches a threshold value of approximately -55mV. This depolarisation results in the opening of some sodium channels, thereby increasing the permeability of the membrane for sodium, while the potassium channels remain closed. The increase in the concentration of Na^+ causes further depolarisation, resulting in an instantaneous increase in the membrane potential, which reaches +30 mV. Afterwards, the process is terminated by the closure of the sodium channels and the subsequent slow opening of the potassium channels, which causes the membrane potential to return to its resting value. Once the resting state is re-established, the permeability for potassium is at its maximum, in contrast to that for sodium, which is at its minimum. This results in hyperpolarisation, whereby the potential reaches more negative values than the resting potential. This mechanism is terminated by the gradual closure of the channels K^+, which brings the membrane potential to its resting value.
Moreover, a refractory period ensues during and immediately following an action potential, during which the neuron is less excitable than in the resting state. The defining characteristic of APs is that they do not increase in amplitude with increasing stimulus intensity; as a result, they are not graded phenomena. When action potentials are generated, it is not the entire axon that is depolarised simultaneously; rather, only a limited area of the membrane is affected at a time. The depolarised zone, described as approximately 1-3mm^2[20], undergoes an inversion of the membrane potential, which generates charge currents that move into adjacent resting regions. These currents trigger new potentials in the zones following the previously depolarised one, which repolarises. Due to the refractory period in which the trigger zone is located, the stimulus can only propagate in one direction. This process continues until it reaches the axon, thus maintaining the intensity of the stimulus.[17][21]

1.3 Electromygraphy signal characteristics

Electromyography (EMG) is an experimental technique that involves the development, recording, and analysis of myoelectric signals. These signals are generated by physiological changes in the state of muscle fiber membranes.[22] Kinesiological EMG is a proven method for studying the voluntary activation of muscles during motor tasks. In contrast, neurological EMG is limited by the artificial nature of the muscle response, which is induced by external electrical stimulation. In addition to biomechanical and physiological studies, EMG is a valuable tool for rehabilitation, medical research, ergonomics and

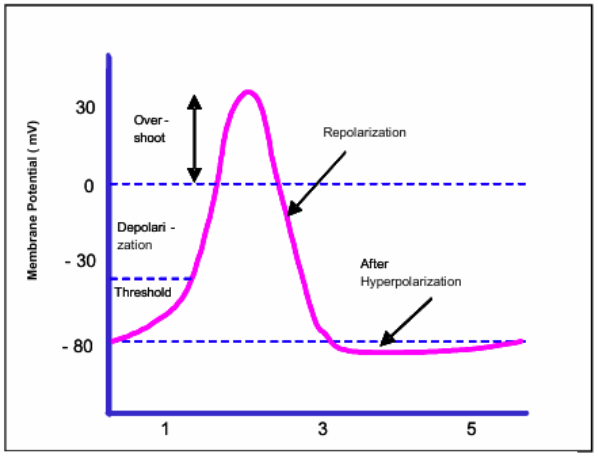

Figure 1.2: The Action Potential.[21]

sports.[21] It allows for the following:

- The measurement of muscle performance;
- The documentation of treatment and training regimes;
- The detection of muscular response to ergonomic studies;
- The analysis to improve sports activities and muscle training.

It should be noted that electromyography is divided into two main categories: surface electromyography (sEMG) and needle electromyography or electroneurography (ENG). Surface EMG involves the acquisition of the signal via surface electrodes, which are placed on the skin. In contrast, ENG involves the use of subcutaneous needle electrodes in direct contact with the muscle. The former method records potentials from a group of motor units, whereas the latter can analyse a single motor unit.
The present study will only consider the superficial EMG, as it is the focus of this work.

The EMG signal is generally understood to be influenced by the action potentials described above. These action potentials represent the sum of the APs of the various fibres that make up a motor unit. The set of potentials in question is known as the Motor Unit Action Potential (MUAP), and its characteristics are dependent on the shape and size of the motor unit and the arrangement of the fibres with respect to the acquisition electrodes. In particular, in a surface EMG, the acquired signal is given by the superposition of all the MUAPs detectable by the electrodes, including MUAPs belonging to different motor units. Consequently, the amplitude and shape of an EMG trace depend on the recruitment of motor units and their firing rate, i.e. the frequency with which each motor unit generates an AP. The resulting signal therefore resembles an 'interference' given by the sum of the various MUAPs detected. However, the activity of the latter is not accurately reflected in the EMG trace due to the presence of the skin, which acts as a low-pass filter.

The unprocessed EMG signal taken during a motor task has a baseline and muscle activation zones. The baseline represents the state of no muscle contraction. It should have a very low amplitude, but this may be altered by the presence of noise. The muscle activation zones, on the other hand, have peaks of variable amplitude. These, due to the variability of MU recruitment, cannot be reproduced between one activation and another.

The signal is therefore processed to try to reduce the presence of noise and randomness in shape.

A sEMG has an amplitude between ± 5000 μV (including athletes) and a frequency content between 5 and 500 Hz. However, the greatest activity is observed between 20 and 250 Hz. This can be observed by analysing the signal power spectrum, which describes the distribution of signal power across the various frequencies. The spectrum is in fact influenced by the activity of the slow twitch MUs, which have a firing frequency between 20 and 125 Hz, and by the activity of the fast twitch MUs, which operate between 120 and 250 Hz. Furthermore, the activity of the larger MUs, which have a low firing frequency of approximately 10-40 Hz, and the activity of the smaller MUs, which have a higher firing frequency of up to 100 Hz, can be distinguished.

1.3.1 Instrumentation

The subject of the analysis represents the signal source. Electrodes act as sensors. Filters, amplifiers and A/D conversion systems belong to the signal manipulation block. Finally, the oscilloscope or digital systems such as PCs or microcontrollers constitute the visualisation block.Figure 1.3 illustrates a potential block representation of an electromyograph.

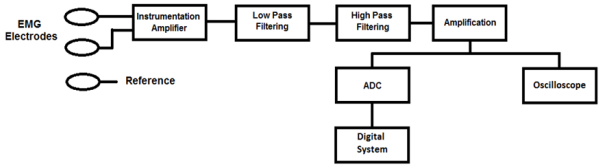

Figure 1.3: A schematic representation of an electromyograph.[23]

Among the potential electrodes that could be utilized in such a study are surface electrodes. These electrodes contact the skin and are non-invasive, thus suitable for superficial muscles. The most commonly used ones are made of silver/silver chloride (*Ag-AgCl*). The *AgCl* layer facilitates the unobstructed transmission of electrical currents from the muscle across the interface between the electrolyte and electrode. This results in a reduction in electrical noise in the measurement compared to equivalent metallic electrodes (e.g., *Ag*). For this reason, *Ag-AgCl* electrodes are employed in over 80% of surface EMG applications.[23]
Electrodes may be gel electrodes, disposable or reusable, which require adequate skin preparation (removal of hair, the correct amount of gel, etc.); or dry electrodes which do not require a gel interface with the skin. These electrodes have a greater mass than the former and, as a consequence, may prove more challenging to affix. However, they are the most commonly used in devices that can be worn independently, and not by a professional, precisely because of the absence of skin preparation.
Furthermore, electrodes are divided into active and passive. The former, which typically fall into the dry category, are equipped with an integrated pre-amplification circuit. This feature serves to mitigate the impact of electrode movement or capacitive coupling, which can result in the generation of parasitic currents. In contrast, the latter require an external amplification circuit.
In order to achieve optimal signal detection, the electrodes must be positioned longitudinally to the muscle, between the motor unit and the tendinous insertion, which are the

areas where the signal is weakest.

The electrodes can be arranged in three distinct configurations:

- Monopolar, only a single electrode is placed on the skin in relation to a reference electrode. A configuration that is straightforward, but susceptible to crosstalk.
- Bipolar, comprises two EMG-detecting surfaces, positioned at a distance of 1-2 cm from each other, with a reference electrode. A differential amplifier is employed to suppress common noise signals and then amplify the difference between the two detecting electrodes. The limitations of the monopolar configuration are eliminated.
- Multipolar, comprises more than two EMG-detecting surfaces with a reference electrode. It reduce crosstalk and noise, thereby enhancing the quality of the EMG signal. In instances where more than two electrodes are utilised, it is necessary to employ more than two differential amplifiers.

Upon detection of the signal by the electrodes, it is transmitted to an instrument amplifier (active electrodes), whose function is to "pre-amplify" the EMG signal, which is naturally weak. The amplifier frequently comprises two stages, with the objective of enhancing the Common Mode Rejection Ratio (CMRR), which is the ratio between the differential and common mode gain and serves as an indicator of the quality of the amplification technique.
The first stage of the amplifier must possess a high input impedance (1-10MΩ)[21] in order to minimise the connection error with the electrodes and any potential imbalance; the second stage is differential and enables the substantial reduction of the common mode noise of the inputs due to acquisition artefacts.

Once the signal has been pre-amplified, it is filtered out, as despite the differential amplifier, noise still has a significant influence. Low-frequency noise is frequently attributed to temperature fluctuations or electrode movement, whereas high-frequency noise may be attributed to nerve conduction or interference from other equipment. The former can be eliminated by a high-pass filter, which has a cut-off frequency below which all frequencies are eliminated. The latter is eliminated by a low-pass filter, which has a cut-off frequency above which all frequencies are removed. The combination of these filters is referred to as a bandpass filter, which retains only the frequencies of interest. In the field of electromyography, it is typical to attempt to retain the frequencies between 5 and 10 Hz and 500 Hz.[23][24]

Following filtration, the EMG signal is amplified once more, with amplification factors of between 500 units (in the case of pre-amplification) and 1000 units (in the absence of pre-amplification, i.e. passive electrodes). The amplification factor may also be increased if the muscles in question exhibit weak responses.
This stage can be achieved with a non-inverting amplifier, whose gain can be set according to the muscle response.

The signal that has been the subject of study and discussion thus far is an analogue signal, which must undergo digitisation in order to be analysed and processed on a computer. The digitisation process was made possible by the Analog to Digital Converter (ADC). In the process of converting an EMG signal into a digital format, it is essential to consider three key specifications: the quantisation, the range of conversion and the

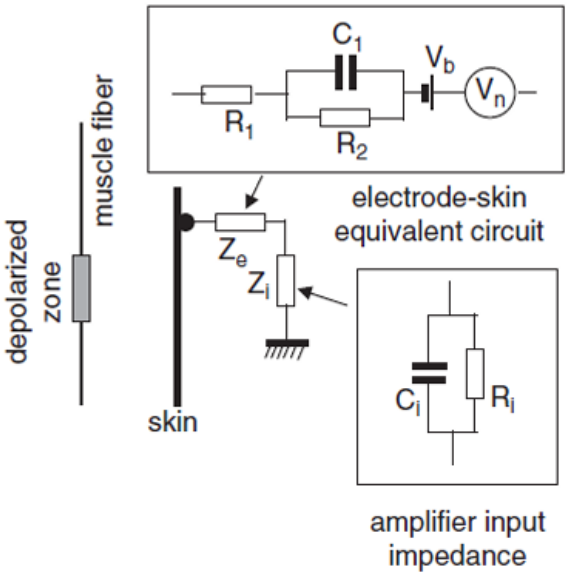

Figure 1.4: Equivalent circuit of an electrode. R_2 and C_1 make up the impedance associated with the electrode-electrolyte interface, and R_1 is the series resistance associated with interface effects and due to resistance in the electrolyte. The generator V_b represents the depolarisation zone of the fibre, while the noise is represented by the quantity V_n.[25]

sampling rate. Quantisation refers to the number of bits that can be used to convert an analog signal into a digital one. The number of quantisation bits is of significant importance, as they determine the ADC's resolution. The range of an ADC is defined as the maximum voltage that can be converted into a digital quantised bits. Sampling rate, on the other hand, is the number of samples that can be converted in one second. The selection of the latter is crucial to prevent aliasing effects, whereby the signal spectrum overlaps. This is elucidated by the Sampling Theorem of Nyquist, which stipulates that the sampling rate must be twice the maximum frequency of the signal. As previously stated, for EMG the majority of the signal power is located between 10 and 250 Hz. Scientific recommendations suggest setting the amplifier band between 10 and 500 Hz[24]. Consequently, a sampling frequency of at least 1000 Hz (double the upper limit of the EMG band) or even 1500 Hz is recommended to avoid signal loss[21].

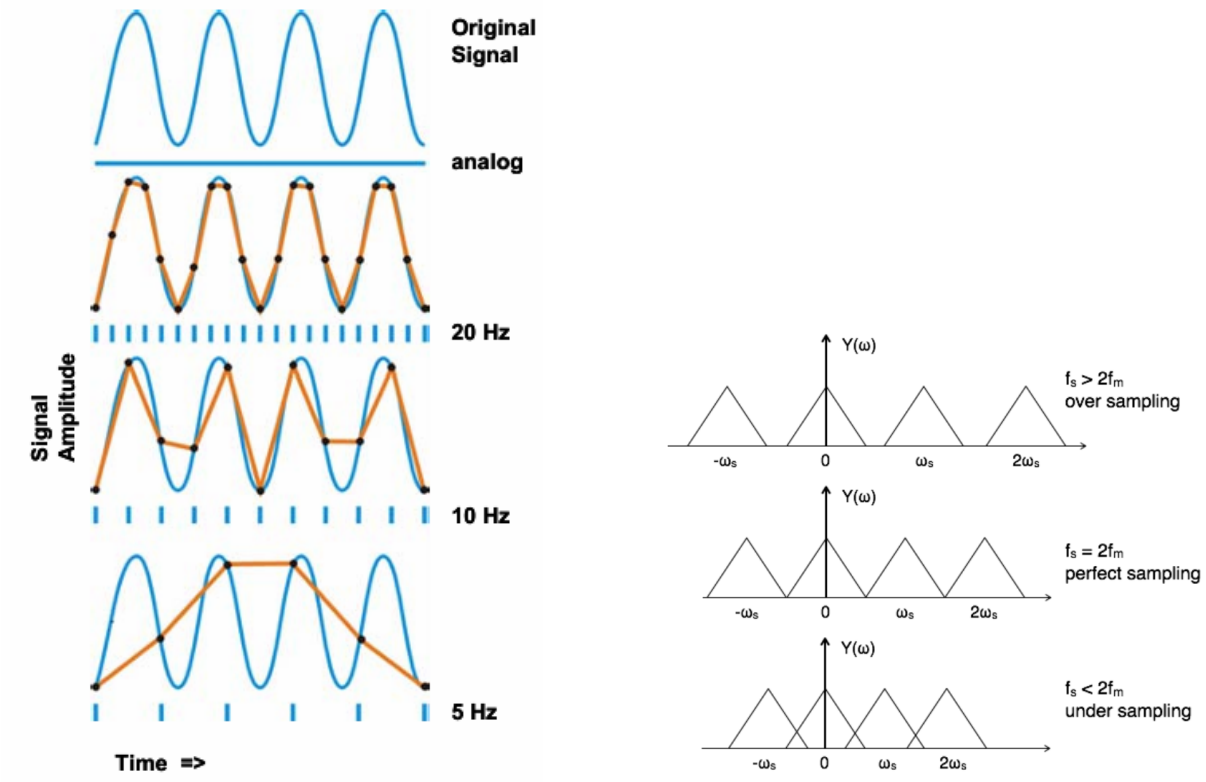

(a) **(b)**

Figure 1.5: a) The impact of ADC sampling frequency on digitised signal. A reduction in the frequency of the signal results in a notable loss of information[21]. b) The aliasing effect is observed when the sampling rate does not respect the Nyquist criterion, resulting in an under-sampling of the signal.

Chapter 2

Material and Methods

This study was conducted in collaboration with Morecognition s.r.l., which provided the wireless device capable of acquiring sEMG signals, and with the University of Turin for the design and execution of the exercise protocol.
A total of twenty subjects, with an average age of 77.05 $\pm$ 11.09 years, were recruited for the analysis of this work. The division and evaluation of the subjects will be described in detail below.

2.1 REMO® device

The REcognition MOvement device (REMO®) is currently manufactured and distributed by Morecognition S.r.l. It was developed by a collaboration between Morecognition and the Italian Institute of Technology in Turin and the San Camillo IRCCS hospital in Venice. The device is designed to be worn easily and is capable of detecting forearm muscle activity during hand movements.
The device was developed with the aim of performing remote upper limb physiotherapy of post-stroke patients. The REMO® device is able to identify electromyographic and inertial signals, which are then used to provide two forms of biofeedback. One of these is proportional to the sEMG signal pattern, while the other is related to the spatial orientation of the device.
The inertial component is provided through the use of an accelerometer, a gyroscope and a tri-axial magnetometer. The myoelectric signal is instead captured via an 8-channel sEMG system, comprising eight dry bipolar electrodes with a diameter of 10 mm and an interelectrode distance of 20 mm. The array is flexible and is attached to a stretchable band, allowing for adaptation to the circumference of the subject's forearm (range between 17 and 27 cm, based on different information about the anatomy of the forearm of men, women and young and elderly subjects). The placement of electrodes over the entire circumference of the forearm ensures that REMO® does not idenitfy signals from a single muscle, but rather from all the muscles in that area. This approach has the potential to reduce crosstalk and enhance the convenience of controlling computer interfaces for rehabilitation purposes.
Furthermore, the device incorporates a processing module comprising an analogue front-end for acquiring the bioelectric signal, a microcontroller and a Bluetooth Low Energy module that enables the sEMG signals to be transmitted to a mobile phone or PC laptop.

The device is powered by an internal lithium polymer battery, which provides approximately 8 hours of battery life in data streaming mode.
The sEMG signals are sampled at a frequency of 2 kHz and then filtered through a bandpass filter between 70 and 500 Hz, after which they are digitised using a 24-bit analog-to-digital converter. Subsequently, the signal is rectified and the root mean square value (RMS) of the rectified signal is calculated utilising a 64 ms window. This signal is then transmitted via Bluetooth to the connected device, where a user interface generates a real-time plot of the processed sEMG, providing feedback representative of the forearm zones under study.

Table 2.1: Technical Specifications of the REMO® Device[26].

Feature	**Specification**
Model	REMO
UDI-DI BASE	805957184REMON4
Classification	Battery-powered system
Housing	Plastic
Power Supply	Rechargeable 3.7V battery
Battery Life	8 hours (full charge)
Charging Time	3 hours
Insulation Class	Class II
Number of Channels	8
Input Dynamic Range	3.3 V
Bandwidth	70:500 Hz
Input Referred Noise Level	$< 2\ \mu V_{RMS}$
Gain	1 V/V
Input Impedance	>90 MΩ over entire bandwidth
CMRR	>96 dB
Output Dynamic Range	0:3.3 V
A/D Converter Resolution	24 bit
Wireless Transmission Mode	BLE
Sampling Frequency	2000 Hz
Dimensions	55 x 60 x 20 mm
Weight	60g
Applied Parts	Type BF
Compatible Operating System	At least Android 8.0 or iOS 15.0

The armband was positioned approximately 5 cm from the olecranon [27] using the SENIAM protocol (Surface ElectroMyography for the Non-invasive Assessment of Muscles)[28], as described in subsection 1.3.1. The Figure 2.2b illustrates the position of the device, which was designed to primarily engage the wrist flexor muscles, specifically the flexor carpi radialis muscle and the flexor carpi ulnaris muscle.
Moreover, Morecognition developed specialized software for monitoring and visualizing the exercises. In particular, video tutorials of the various exercises were produced for this study and uploaded to the application. Subsequently, the subjects were permitted to select the exercise to be performed on each occasion. This was accompanied by the demonstration video and a pendulum, which was capable of scanning the rhythm of each repetition according to the duration of the total exercise.[27][29][30]

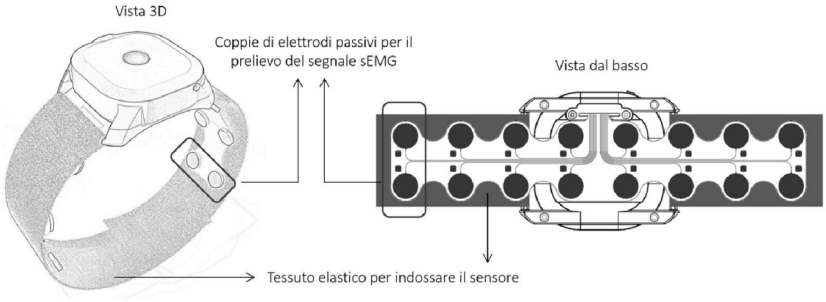

Figure 2.1: The REMO® structure

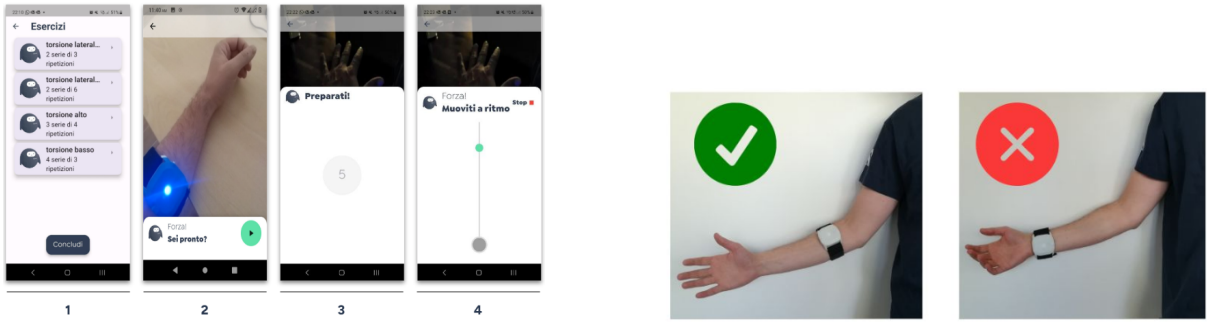

(a) **(b)**

Figure 2.2: a)User interface of REMO® app. b)The correct positioning of the device[26]

2.2 Exercise protocol

The REMO® system has been designed to assist the rehabilitation of post-stroke patients, allowing them to engage in daily exercise from home with remote monitoring by qualified professionals. The exercise protocol has been chosen based on the Fugl-Meyer (FM) Assessment scale. The Fugl-Meyer Assessment (FMA) is a widely used tool in post-stroke rehabilitation, being recognised as one of the most comprehensive measures of motor impairment in this field.
The Fugl-Meyer scale is divided into five categories: motor function, sensory function, balance, joint range of motion and joint pain. Each category contains several items, each of which is associated with a scale from 0 to 2 (0 = cannot perform, 1 = performs partially, 2 = performs fully). The objective of this study is to perform a binary classification of frailty based on the motor activity of the upper limb. Therefore, it was decided to use only the category related to motor function for the assessment. This category includes items measuring movement, coordination and reflex action on the shoulder, elbow, arm, wrist, hand, hip, knee and ankle. For the purposes of this work, the focus was therefore on the wrist and hand fields.[31]
The tables below present the rating scale for wrist and hand range of motion (ROM).

Table 2.2: FM scale exercise protocol for wrist ROM.[32]

B. WRIST Support may be provided at the elbow to take or hold the starting position, no support at wrist, check the passive range of motion prior to testing		**None**	**Partial**	**Full**
Stability at 15° dorsiflexion Elbow at 90°, forearm pronated, shoulder at 0°	- Less than 15° active dorsiflexion - Dorsiflexion at 15°, no resistance tolerated - Maintains dorsiflexion against resistance	0	1	2
Repeated dorsiflexion / volar flexion Elbow at 90°, forearm pronated, shoulder at 0°, slight finger flexion	- Cannot perform volitionally - Limited active range of motion - Full active range of motion, smoothly	0	1	2
Stability at 15° dorsiflexion Elbow at 0°, forearm pronated, slight shoulder flexion/abduction	- Less than 15° active dorsiflexion - Dorsiflexion at 15°, no resistance tolerated - Maintains dorsiflexion against resistance	0	1	2
Repeated dorsiflexion / volar flexion Elbow at 0°, forearm pronated, slight shoulder flexion/abduction	- Cannot perform volitionally - Limited active range of motion - Full active range of motion, smoothly	0	1	2
Circumduction Elbow at 90°, forearm pronated, shoulder at 0°	- Cannot perform volitionally - Jerky movement or incomplete - Complete and smooth circumduction	0	1	2
	TOTAL B (max 10)			

Table 2.3: FM scale exercise protocol for hand ROM.[32]

C. HAND support may be provided at the elbow to keep 90° flexion, no support at the wrist, compare with unaffected hand, the objects are interposed, active grasp				
Mass flexion From full active or passive extension		0	1	2
Mass extension From full active or passive flexion		0	1	2
GRASP				
a. Hook grasp flexion in PIP and DIP (digits II-V), extension in MCP II-V	- Cannot be performed - Can hold position but weak - Maintains position against resistance	0	1	2
b. Thumb adduction 1-st CMC, MCP, IP at 0°, scrap of paper between thumb and 2-nd MCP joint	- Cannot be performed - Can hold paper but not against tug - Can hold paper against a tug	0	1	2
c. Pincer grasp, opposition pulpa of the thumb against the pulpa of 2-nd finger, pencil, tug upward	- Cannot be performed - Can hold pencil but not against tug - Can hold pencil against a tug	0	1	2
d. Cylinder grasp cylinder shaped object (small can) tug upward, opposition of thumb and fingers	- Cannot be performed - Can hold cylinder but not against tug - Can hold cylinder against a tug	0	1	2
e. Spherical grasp fingers in abduction/flexion, thumb opposed, tennis ball, tug away	- Cannot be performed - Can hold ball but not against tug - Can hold ball against a tug	0	1	2
	TOTAL C (max 14)			

The protocol comprised twelve exercises, which were superimposed. Each of the aforementioned exercises was performed while wearing a REMO device, which had been previously connected to the application on a smartphone in order to record the myoelectric activity of the various exercises.

2.3 Frailty assessment

Each subject was evaluated to determine the presence of frailty.
The criteria used to assess frailty were Fried's phenotype and TFI (section 1.1). Hence, subjects performed motor tasks, including a timed walk test which was conducted over a distance of 4.5 m and six hand grip strength assessments (the body district concerned in this study) using a dynamometer, with three assessments per arm in an alternating manner. The latter measurement is related to the subject's gender and their body mass index (BMI).
They then answered several questions on the Physical Activity Scale for the Elderly (PASE)[33] to assess their level of sedentariness, and questions from the Center for Epidemiologic Studies Depression Scale (CES-D Scale)[34] to quantify the energy loss required by the Fried phenotype.
Subsequently, the second part of the TFI questionnaire was completed, comprising socio-demographic questions and covering the subject's medical history. This was done in order to obtain a comprehensive picture.

2.4 Dataset

The dataset comprises electromyographic signals obtained from the armband during the twelve exercises, each comprising six repetitions. During execution, subjects viewed a pendulum on the app, which marked the time of each repetition.
A total of twenty subjects were recruited. For each subject, the exercises were performed and the corresponding signals were taken for each upper limb. In this work, the acquisitions of each limb were considered independently, without reference to or consideration of belonging to the same individual. Consequently, the total dataset comprises forty exercise sets with their respective repetitions. Given that each set comprises twelve exercises, the total number of acquisitions is 480, regardless of the subjects.
However, due to issues with storage and/or connectivity between the device and the smartphone, some subjects have incomplete data for certain exercises. Some subjects did not record any data at all, despite it being saved in the cloud of the device. Consequently, the final dataset has fewer signals.
It should be noted that, as the objective of this study is to classify subjects based on the features extracted from individual acquisitions, the valid exercises of subjects with technical issues were retained. Consequently, the final dataset comprises a total of 441 exercise acquisitions from the various subjects, each containing six repetitions.

2.5 Pre-processing

Firstly, in order to familiarise with the signals, they were plotted, distinguishing each acquisition channel and exercise through the different subjects. Secondly, in order to gain

a deeper understanding, the Power Spectral Density (PSD) was also analysed.

2.5.1 Power Spectral Density

The PSD was calculated using the Welch's method, whereby the signal was divided into overlapping segments, the periodogram was calculated for each segment and the periodograms were averaged. The Hamming window was used, as it represents a compromise between resolution and the power leakage. The window length was calculated as half of the signal in order to be a power of two, as is typically used in these algorithms. While the sampling frequency is set to 2000 Hz and the number of points to overlap between segments is zero.

2.5.2 Filtering

As previously stated, the signals recorded by REMO® were already filtered between 70 and 500 Hz, hence the foundamental band of an EMG was already selected. The significant band for an EMG signal is in fact between 10 Hz and 500 Hz. However, high-pass filters are often applied with frequencies around 20 Hz or more to attenuate the effect of motion artefacts, which is a very influential factor in a sampling system used in this study. Therefore, no additional filters were employed at this stage. In particular, the necessity for a notch filter to reduce network interference was negated by the fact that REMO®, a wireless device, is not susceptible to network frequencies (equal to 50 - 60 Hz in Europe).

2.5.3 Rectification and calculation of the Root Mean Square value

The next step should had been the rectification, by calculating the absolute value of the signals. This approach yields numerous advantages, including enhanced signal interpretation, the ability to calculate standard parameters such as mean, area subtended by the signal, and maximum value. However, this step was already implemented by the armband, which is why this step was also omitted.
Furthermore, the REMO® algorithm also computes the Root Mean Square (RMS) over a window of 64 ms. This process results in a smoothing of the sEMG signal, whereby the replicable components are isolated from the non-replicable components, which are often the result of noise.

2.5.4 Normalisation

Subsequently, the signals were normalised in order to decrease differences between the signals where possible. Acquiring different subjects with different physiological characteristics would have resulted in significant variations. Even an error in electrode placement between subjects could have led to variations not inherent to the analysis carried out in this work. Differences in skin characteristics would also have affected the results. Consequently, it was deemed appropriate to normalise the data in order to reduce inter-subject variability and facilitate the comparison and analysis of signals from different individuals[35].

As the subjects had not previously performed the exercises required to obtain the signals necessary for calculating the maximum voluntary contraction (MVC) with respect to wrist and hand movements, the acquisition set was used as a reference. This resulted in the selection of one of the exercises performed during the acquisition set as the MVC. Given the subjects' exercises relating to wrist and hand movements, it was deemed appropriate to choose two different exercises for normalisation.
With regard to the movements relative to the wrist (Table 2.2), the second exercise of the set was chosen as the reference exercise, namely "Repeated dorsiflexion/volar flexion with elbow at 90°". This is one of the exercises carried out that best represents the maximal contractions of the muscles involved. Another valid exercise for this purpose would have been the first of the set: "Stability at 15° dorsiflexion with elbow at 90°". However, due to problems occurring during the acquisition and saving of the data, some subjects did not present this exercise, unlike the second one, which was present in all subjects. For this reason, it was chosen as the reference exercise for the normalisation of wrist movements. In contrast, in order to normalise the exercises relating to hand movement (Table 2.3), all the exercises performed during the acquisitions could have been used, as they are all able to represent the contraction of the muscles involved. The final exercise in the set, "Spherical grasp", was therefore selected as the most appropriate exercise, as it was present in all subjects and comparable to the hand grip exercise with dynamometer, which is frequently employed in the literature as one of the possible MVC exercises for the hand[36].

2.5.5 Envelope

Following the implementation of the normalization process, the envelope was calculated. Consequently, an IIR (infinite impulse response) filter was implemented. The IIR filter was selected due to its lower order, which results in a lower latency than that of the FIR filter (finite impulse response filter). Nevertheless, IIR filters exhibit non-linear phase characteristics that can distort the signal's morphology. However, this characteristic does not influence EMG signals, which have a casual morphology and are non-replicable. Accordingly, a Butterworth low-pass filter was implemented, which is the only filter that has a flat frequency response in the passband. A fourth-order filter was selected to achieve a more significant attenuation (80 dB/decade). The cut-off frequency was set equal to 10% of the sampling frequency (2000 Hz), resulting in a cut-off frequency of 200 Hz. This decision was taken as the signal had already been subjected to the smoothing effect of the RMS calculation, and a lower envelope frequency would have resulted in a number of disadvantageous circumstances. One consequence of this approach would have been an overestimation of the instants of activation, with the onset and offset being anticipated and postponed, respectively. This would have been due to a combination of factors, including a lower filter response and the cutting off of certain components of the high-frequency EMG signal, which are characteristic of rapid changes in muscle activation. Furthermore, selecting a cutoff frequency that was too low would have resulted in an excessive damping of the signal, which would have made it less dynamic and therefore unrepresentative.
Therefore, once the optimal cutting frequency has been identified, the coefficient of the digital filter was calculated and the envelope was computed for each channel of acquisition.

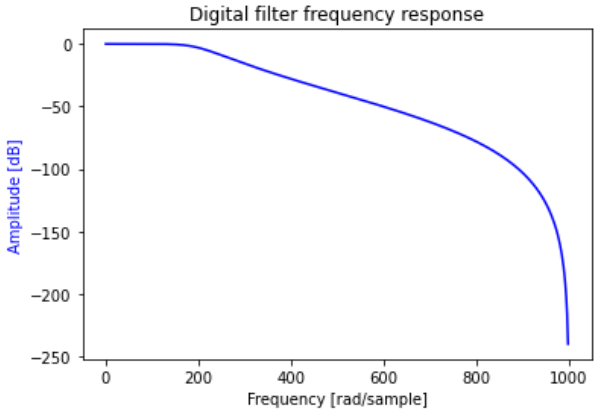

Figure 2.3: Frequency response of Butterworth low-pass filter.

2.6 Implementation of Signal to Noise Ratio

The signal-to-noise ratio (SNR) is a measure that quantifies the quality of a signal, specifically how much the noise component affects the overall signal. A lower SNR value indicates a greater influence of noise.
The EMG signal is defined as a random signal. This randomness is a consequence of a number of factors, including the irregular firing rate, the random response of the individual muscle units (MUs), and the differences in characteristics between the latter. Indeed, it was claimed that the electromyographic signal appeared to be analogous to "interference" due to the superimposition of the various MU activities. Furthermore, it was asserted that the EMG signal could be characterised by a considerable amount of noise, resulting from motion artefacts or suboptimal electrode positioning, which are also unpredictable and irregular factors.
In order to account for the stochastic nature of both the signal and the noise, the calculation of SNR incorporates the ratio of signal power to noise power.
In essence, the overall signal can be defined as follows:

$$x(t) = s(t) + n(t)$$

as the sum of muscle activity and noise.
The SNR of a signal and noise that are considered to be random processes is implemented as follows:

$$SNR_{dB} = 10 \cdot \ log_{10} \frac{P_s}{P_n}$$

The power of the individual components that comprise the overall signal, $x(t)$, was calculated.
In order to identify the real signal, $s(t)$, and the noise, $n(t)$, we focused on the individual repetitions present in each signal. This involved identifying windows that contained each individual repetition, identifying the real signal and noise within them, and then calculating the signal-to-noise ratio.
The SNR was subsequently calculated by averaging the individual values derived for each repetition. This approach was taken in order to obtain a more representative estimate of the signal's overall quality, and because focusing on each repetition enabled more accurate

identification of the noise.

2.6.1 Identification of repetitions

Each exercise comprises six repetitions. In order to identify each, an algorithm was developed to identify the largest peak of each activation interval and then centralise it within a window, which was then used to calculate the signal-to-noise ratio.
In order to identify the peaks, a window size equal to one sixth of the signal length was initially set, ensuring that each window contained an entire repetition.
Subsequently, the signal was divided by sliding segments as long as the window, with a step size equal to half the window. The mean and standard deviation of each segment were calculated in order to determine the threshold for peak identification.

$$threshold = mean + std$$

Peaks were identified by imposing a threshold and a prominence equal to half the difference between the maximum and minimum value of the current segment. Of those identified, the maximum was taken and imposed as the centre of the signal activation window. Windows of a duration shorter than the imposed time limit, equal to half the activation window, were then eliminated, while the others were saved for the calculation of the signal-to-noise ratio (SNR).

2.7 Feature extraction

In order to train a classifier for the recognition of fragile subjects, several features were implemented and extracted with reference to those most frequently used in the literature. The fetaures listed below were calculated by processing the signal in two different ways.

- **Features Dataset 1** The features for each previously identified activation window were calculated. The values obtained were then averaged together to obtain a feature set for each signal.
- **Features Dataset 2** Prior to the calculation of the features, the various activation windows of each signal were first averaged.

The decision was reached to average the features with the intention of reducing the potential variability that might have been present between the various repetitions, thereby obtaining more stable values.
The extracted features are presented in the following list.

- **Root Mean Square (RMS)**[37][38][39][40]
  This feature characterises the signal amplitude, and the computational speed and efficiency are high.
  $$\text{RMS} = \sqrt{\frac{1}{N}\sum_{i=1}^{N} x_i^2}$$
- **Variance (VAR)**[41][40]
  It measures the desnidty power of the EMG signal.
  $$\text{VAR} = \frac{1}{N}\sum_{i=1}^{N}(x_i - \mu)^2$$

Algorithm 1 Identification of repetitions

Parameters
▷ Initialisation
$window\_size \leftarrow \text{len}(signal)/6$
$step\_size \leftarrow window\_size/2$
$time\_limit \leftarrow \text{len}(window\_size)/2$
▷ Execution
for $j \leftarrow 0$ to $\text{len}(signal) - window\_size$ by $step\_size$ **do**
    if $j + window\_size > \text{len}(signal)$ **then**
        $segment \leftarrow signal[j:]$
    else
        $segment \leftarrow signal[j : j + window\_size]$
    end if
    ▷ Calculation of the mean and standard deviation for each segment
    $std\_segment \leftarrow \text{std}(segment)$
    $mean\_segment \leftarrow \text{mean}(segment)$
    ▷ Calculation of the threshold
    $threshold \leftarrow mean + std\_segment$
    ▷ Minimum and maximum calculations for prominence
    $max\_segment \leftarrow \max(segment)$
    $min\_segment \leftarrow \min(segment)$
    ▷ Peak computation
    $peaks \leftarrow \text{find\_peaks}(segment, \text{height} = threshold, \text{prominence} = max\_segment - min\_segment)/2)$
    ▷ Finding of the maximum peak
    $max\_peak \leftarrow \max(peaks)$
    ▷ The window is centred on the maximum peak
    $start\_window \leftarrow max\_peak - step\_size$
    $end\_window \leftarrow max\_peak + step\_size$
    $window \leftarrow signal[start\_window : end\_window]$
    if $\text{len}(window) > time\_limit$ **then**
        activation_intervals.append($start\_window, end\_window$)
    else
        continue ▷ If the window is shorter than the specified time limit, it will not be saved
    end if
end for
return *activation_intervals*

- **Standard Deviation (STD)**

$$\text{STD} = \sqrt{\text{VAR}} = \sqrt{\frac{1}{N}\sum_{i=1}^{N}(x_i - \mu)^2}$$

- **Mean Absolute Value (MAV)**[41][37][38][40]
  It is employed for the purpose of detecting and measuring muscle contraction.

$$\text{MAV} = \frac{1}{N}\sum_{i=1}^{N}|x_i|$$

- **Waveform Length (WL)** [42][41][37][38][39][40]
  This feature can be regarded as the sum of the waveform along the segment. It can be used to indicate the degree of variation in the EMG signal.

$$\text{WL} = \sum_{i=1}^{N-1}|x_{i+1} - x_i|$$

- **Willison Amplitude (WAMP)**[41][37][39][40]
  The WAMP count is incremented for each change in the amplitude of the EMG signals that exceeds a defined threshold. This parameter serves as an indicator of the potential range of movement and is, therefore, a principal measure of muscle contraction.

$$\text{WAMP} = \sum_{i=1}^{N-1} f(|x_i - x_{i-1}|)$$

$$f(x) = \begin{cases} 1 & \text{if } x > \text{threshold} \\ 0 & \text{if } x < \text{threshold} \end{cases}$$

  where f is the indicator function and *threshold* is a predefined threshold.

- **Integrated s-EMG (IsEMG)**[37]
  It is employed to ascertain the intensity or extent of muscle activity over a specified period. The greater the value of IsEMG, the more intense the muscle activity during the specified time interval.

$$\text{IsEMG} = \sum_{i=1}^{N}|x_i|$$

- **Simple Square Integral (SSI)**[37]
  It reflects the area under the curve, yet assigns greater significance to the components exhibiting high amplitudes. It can be used as an EMG signal energy.

$$\text{SSI} = \sum_{i=1}^{N} x_i^2$$

- **Activation (ACT)**
  It measure the activation's length in samples. It is calculated as the difference between the final and initial times.

$$\text{ACT} = t_N - t_0$$

- **Mean Frequency (f-Mean)**[40]
  This function computes a weighted average of the signal frequency based on the power spectral density.
  $$f_{\text{Mean}} = \frac{\sum_{i=1}^{N} f_i P(f_i)}{\sum_{i=1}^{N} P(f_i)}$$
  where $P(f_i)$ is the Power Spectral Density at f_i frequency.

- **Median Frequency (f-Median)**[40]
  It represents a frequency at which the EMG power spectrum is divided into two regions with equal area, but it is also defined as half of the total power.
  $$\sum_{i=1}^{k} P(f_i) = \frac{1}{2} \sum_{i=1}^{N} P(f_i)$$
  where $P(f_i)$ is the Power Spectral Density and f_k is the median frequency.

- **Second order autoregressive coefficient (AR2)**[39][40]
  The coefficients are capable of capturing the temporal dynamics of the signal, which renders them particularly useful for the distinction between different muscle conditions.
  $$x_t = \phi_1 x_{t-1} + \phi_2 x_{t-2} + \epsilon_t$$
  where ϕ_1 and ϕ_2 are the second order autoregressive coefficients and ϵ_t is the error term.

- **Sixth order autoregressive coefficient (AR6)**[39][40]
  $$x_t = \phi_1 x_{t-1} + \phi_2 x_{t-2} + \cdots + \phi_6 x_{t-6} + \epsilon_t$$
  where ϕ_1 and ϕ_2 are the sixth order autoregressive coefficients and ϵ_t is the error term

- **Slope Sign Changes (SSC)**[38][40]
  This refers to the number of times the signal slope undergoes a change in sign over a specified period of time. This feature may be beneficial in the context of capturing rapid changes in the sEMG signal, such as spikes or rapid transitions.
  $$SSC = \sum_{i=2}^{N-1} [((x_i - x_{i-1})(x_{i+1} - x_i) < 0)]$$

- **Average Amplitude Change (AAC)**[37][39]
  It is focused on the average magnitude of amplitude change, without consideration of direction. The AAC can provide information on the variability or overall magnitude of change in the signal over time.
  $$\text{AAC} = \frac{1}{N-1} \sum_{i=1}^{N-1} |x_{i+1} - x_i|$$

- **Entropy (ENTR)**[43]
  It reflects the complexity or randomness of the EMG signal.
  $$\text{ENTR} = -\sum_{i=1}^{N} p_i \log_2(p_i)$$
  where p_i is the probability associated with the value x_i.

- **Crest Factor (CREST)**
  This feature enables the asymmetry and waveform of the signal to be identified.

$$\text{CREST} = \frac{\max(|x|)}{\text{RMS}}$$

- **Kurtosis (KURT)**[38]
  This indicates the degree of concentration of the data around the mean. A kurtosis greater than zero indicates a more "sharp" distribution (with higher peaks and heavier tails) than the normal distribution, while a kurtosis less than zero indicates a more "flat" distribution (with less pronounced peaks and lighter tails). In sEMG, a higher kurtosis may be indicative of a greater concentration of signal energy in higher peaks, which could correspond to more intense or faster muscle contractions.

$$\text{KURT} = \frac{1}{N}\sum_{i=1}^{N}\left(\frac{x_i - \mu}{\sigma}\right)^4$$

- **Skewness (SKEW)**[38]
  Skewness is a measure of the asymmetry of a distribution of data with respect to the mean. A positive skewness indicates that the distribution extends to higher values, while a negative skewness indicates that the distribution extends to lower values. In the sEMG, a positive skewness may indicate a tendency for higher values during muscle contractions than during rest, while a negative skewness may indicate the opposite.

$$\text{SKEW} = \frac{1}{N}\sum_{i=1}^{N}\left(\frac{x_i - \mu}{\sigma}\right)^3$$

where μ is the mean value and σ is the standard deviation of the signal $x(t)$.

2.7.1 Statistical test evaluation

Once the features had been calculated, statistical tests were performed to assess their ability to discriminate between the two classes (fragile/non-fragile).
Statistic tests are classified as either parametric or non-parametric tests. Parametric tests are based on the assumption that the samples have a normal distribution and homogeneous variances. These tests are statistically powerful, as they afford a greater probability of correctly rejecting an erroneous statistical hypothesis. The most renowned and pervasive of these is the Student's t-test. In contrast, non-parametric tests do not require any specific distribution, which renders them considerably more versatile. However, it should be noted that the use of a non-parametric test, when a parametric one would be more appropriate, may result in a notable decline in performance and statistical validity, thereby increasing the probability of error.
In order to idenitify which test was most appropriate, the distribution of the present data was evaluated. Subsequently, the distribution graph was analysed, and the Shapiro-Wilk test was also performed, which is based on the correlation between the data and the corresponding normal scores. This test was selected for evaluation of the data distribution due to its superior power compared to other tests and its frequent recommendation for testing the normality of data.[44]
The null hypothesis of the Shapiro-Wilk test postulates that the data originate from

populations with a normal distribution. The null hypothesis is accepted when the p-value is greater than 0.05.
Upon analysis of the available data, both for frail and non-frail subjects, a p-value of less than 0.05 was obtained, indicating that the null hypothesis is rejected. As a result of the lack of a normal distribution, parametric tests are not applicable, which is why non-parametric tests were employed.
The objective of these tests is to compare two independent groups, comprising fragile and non-fragile subjects, with continuous variables on an interval or rational scale due to the nature of the implemented features. Consequently, the most appropriate statistical test for the present case, as evidenced in the literature, is the Mann-Whitney U-test, which compares the medians of the two groups[45]. In comparison to the Student's t-test, the power of this method is nearly 95% even when utilising a modest sample size.
The null hypothesis (H_0) assumed in this test is that the two medians coincide, hence indicating that the distributions are equal. If the null hypothesis is rejected in favour of the alternative hypothesis (H_1), it can be concluded that there is sufficient statistical evidence to suggest that the distributions of the two populations differ in terms of position, dispersion or shape. Consequently, in the present study, rejecting the null hypothesis would indicate a significant difference in the feature sets for frail and non-frail subjects. This would imply that the implemented features are able to discriminate the presence of frailty.

2.8 Classifier development

Once a dataset of features had been created, we proceeded with the implementation of an automatic classifier for the recognition of frailty.
The first class, designated as 0, was assigned to the features calculated on non-fragile subjects, while the second class, designated as 1, was assigned to the features belonging to fragile subjects.
The subsequent stage of the process involved the division of the dataset. A random division of the dataset was selected to form training set and test set. This approach was selected to reduce the computational cost, which would otherwise be higher using alternative methodologies. Furthermore, it facilitates the generalisation of the model, thereby avoiding overfitting and reducing the risk of selection bias. Additionally, the relatively small size of class 1 in comparison to class 0 would have resulted in underfitting using stratified sampling, as this class would have been underrepresented in the training set, and the model would not have had sufficient samples from class 1 for training.
To achieve a balanced distribution between the training set (TRS) and the test set (TS), it was decided to randomly insert half of the data from class 1 (the least numerous class) and the same amount of data from class 0 into the TRS. This ensures that both classes are represented equally during the training phase. The remaining data from both classes were entered into the TS for model evaluation purposes.

2.8.1 Dimensionality reduction

In order to facilitate classification and decrease the size of the feature dataset, the potential of Principal Component Analysis (PCA) was evaluated. This is an unsupervised technique, the objective of which is not to optimise classification per se, but rather to reduce the size of the data set. In order to perform a dimensionality reduction, a new feature space is

selected. PCA attempts to identify a coordinate system that can explain the variance of the data. This is achieved by performing a linear mapping of the data, with the aim of decreasing the mean square error by removing any dependencies and noise. One limitation of PCA is that it does not consider the information contained in the features. Rather, it identifies the directions in which there is maximum variance, which may not necessarily correspond to the directions in which the information is most discriminated.
Consequently, the use of PCA allows only the most significant principal components to be retained, reducing the number of features considered, decreasing noise and redundant information, and decreasing dimensionality reduces the risk of overfitting.

Prior to the application of PCA, the data underwent standardisation, whereby they were transformed to have a mean of zero and a variance of one.

$$X_{std} = \frac{x - \mu}{\sigma}$$

Standardisation is a fundamental step in the process, as it allows the various features to be compared as they are now projected on the same scale. Furthermore, this approach ensures that the principal components that are to be calculated will not only reflect variables with larger scales.
The next step is to calculate the covariance matrix. For a dataset with n samples and p variables, the dataset can be represented as a X matrix of size $n \times p$. The covariance matrix Σ is a matrix of dimension $p \times p$ whose elements, denoted by σ_{ij}, represent the covariance between the variables i and j.

$$\Sigma = \frac{1}{n-1} \cdot (X - \mu)^T (X - \mu)$$

In this context, the vector μ represents the average values of the variables.
Once the matrix Σ has been calculated, its eigenvalues λ and eigenvectors υ, representing the amount of variance of each principal component and their direction, respectively, are calculated.

$$\Sigma\upsilon = \lambda\upsilon$$

At this juncture, the eigenvalues are ordered in descending sequence along the vector W, and the eigenvectors corresponding to the eigenvalues and degrees represent the directions of the principal components with the highest variance.
The original data are then projected onto the new principal components in order to reduce the dimensionality of the data set.

$$Z = X_{std}W$$

In order to ascertain the optimal number of principal components for incorporation into the classifier development process, a k-fold cross-validation procedure was conducted, with *k=5*. In this process, the dataset is divided into k smaller sets, with *k-1* being used for training and the remaining set for validation. This approach allows for the testing and assessment of a greater number of parameters, including the number of principal components. The model exhibiting the optimal performance and shortest computing time is then saved with the corresponding parameters, which are subsequently employed for the testing phase.
By employing this methodology, it is feasible to conduct numerous tests for comparison,

which may elevate the computational costs, but prevents overfitting of the classifier. This methodology enables the execution of a validation process without the necessity of dividing the original, already limited, dataset into distinct training, validation, and testing subsets. As a result, the number of samples used for training would be considerably diminished.

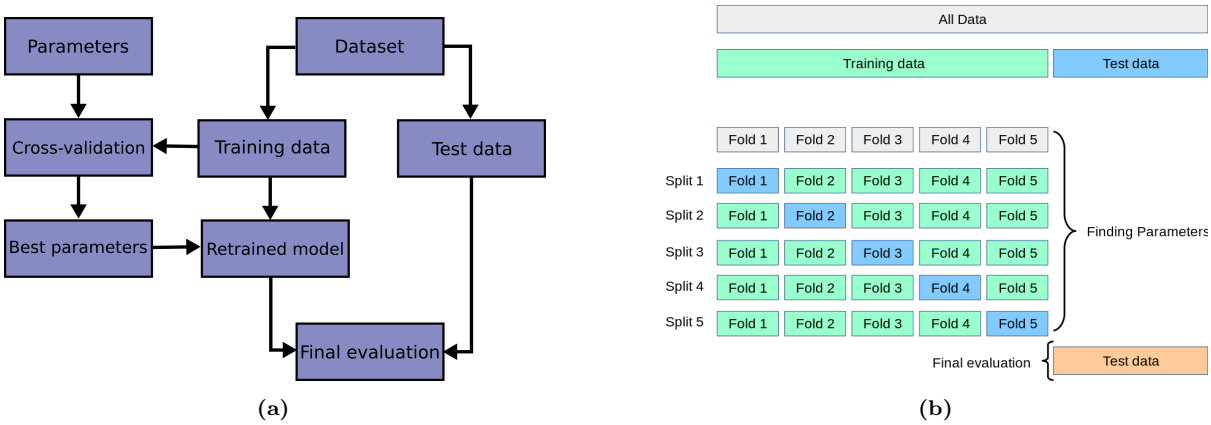

Figure 2.4: a) The classifier training flowchart, b) k-fold cross-validation working diagram.[46]

2.8.2 Support Vector Machine

The Support Vector Machine (SVM) is a machine learning technique that has gained considerable popularity as a classification algorithm, being employed in a wide range of fields. In numerous studies, it has been used to recognise hand movements, and more generally it is a popular tool in the field of pattern recognition [47]. For these reasons, it was selected as the classification tool in this analysis.

The SVM was developed with the objective of creating a hyperplane for separating data that cannot be separated linearly. This is achieved by mapping features into a higher-dimensional space, called Hilbert space[48], using non-linear kernel functions. The use of non-linear kernels greatly aids the algorithm in learning and generalisation[49].
The training of an SVM involves solving an optimisation problem in which the kernel function is able to create linear contours using non-linear transformations. The set used for training an SVM is defined as follows:

$$(x_1, y_1), ..., (x_m, y_m) \in \mathbb{R}^N \times \{-1, +1\}$$

In this context, x_i represents the input value, while y_i represents the respective class. In the event that the aforementioned inputs are not linearly separable, non-linear transformations are introduced from the input space to that of the higher-dimensional features, where the data will be linearly separable.

$$\Phi : \mathbb{R}^N \mapsto \mathbb{R}^M$$

The hyperplane is a decision boundary that separates the two classes in a feature space and can be represented as follows:

$$\omega \times \Phi(x) + b = 0$$

where $\omega \in \mathbb{R}^M$ and $b \in \mathbb{R}$.
Support vectors represent the most proximal data points to the hyperplane, which plays a pivotal role in determining the hyperplane and margin, which is the distance between the support vectors and the hyperplane. In order to construct the hyperplane in a way that allows for maximum separation and minimises error during the training phase, an attempt is made to solve what is known as a quadratic programming problem (QP).

$$min_{\omega,b}\frac{1}{2} \parallel \omega \parallel^2 + C\sum_{i=1}^{m}\xi_i$$

$$y_i(\omega \times \Phi(x_i) + b) \geq 1 - \xi_i$$

with $i = 1, ..., m$.
The former creates maximum margins of separation between classes, whereas the latter imposes an upper limit on the potential for error in training. The presence of error is unavoidable, particularly in the presence of noise. However, limiting the extent of error can help to prevent overfitting [50].
Consequently, if the data is challenging to distinguish directly, the *kernel* function is employed to achieve this separation. In fact, *kernel* is a mathematical function which maps the input data points into the new high-dimensional space.

$$F(\alpha) = \sum_{i=1}^{m}\alpha_i - \frac{1}{2}\sum_{j,k=1}^{m}\alpha_j\alpha_k y_j y_k K(x_j, x_k)$$

subject to

$$\sum_{i=1}^{m} y_i\alpha_i = 0 \quad C \geq \alpha_i \geq 0 \ , \ i = 1, ..., m$$

where $K(x_j, x_k)$ is the kernel function, which can be of different types. The most popular kernels are: linear $K(x_i, x_j) = x_i^T x_j$; polynomial $K(x_i, x_j) = (\gamma x_i^T x_j + r)^d \ , \ \gamma > 0$; radial basis function (RBF) $K(x_i, x_j) = e^{-\gamma\|x_i - x_j\|^2)} \ , \ \gamma > 0$ and sigmoid $K(x_i, x_j) = tanh(\gamma x_i^T x_j + r)$ [51].

In order to enhance the efficacy of the classifier, it is essential to select two primary parameters with precision. The first of these parameters is C, which represents the cost of the penalty. The value of C affects the accuracy of the SVM. A high C value allows for high accuracy in the training phase, but lower accuracy in the testing phase. Conversely, a low C value causes the accuracy during training to drop significantly, rendering the model useless. On the other hand, the parameter γ affects the partitioning result in the feature plane. A high value of γ can result in overfitting, whereas a low value of γ can lead to underfitting [49].
Since the value of these parameters affects the classification result, it was deemed appropriate to include them in the cross-validation described above, along with the evaluation of the number of independent components, in order to identify the optimal combination of these parameters in terms of accuracy. The optimal parameters were identified by comparing the various kernels listed above and selecting the solution with the highest performance.

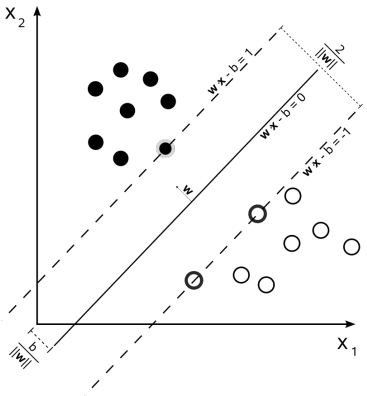

Figure 2.5: The following example illustrates the use of linear separation with SVM.

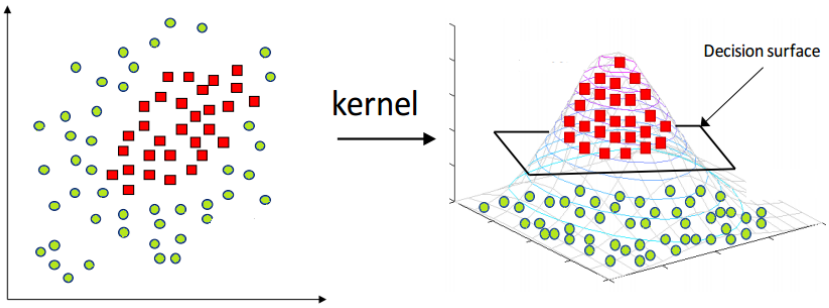

Figure 2.6: The image below illustrates an instance where two data sets are not linearly separable. However, in three-dimensional space, the data set is linearly separable by a three-dimensional hyperplane.

2.8.3 Performance evaluation metrics

The evaluation of performance is a crucial aspect of any assessment process.
In order to assess the quality of the classifier's models, a confusion matrix (CM) was first created. This allows one to compare and visualise the performance of the algorithm within a supervised problem, emphasising the percentages of correctly classified and incorrectly classified instances.
The table contains the actual classification of the data on the rows, while the columns contain the class predicted by the model.

In this study, the terms designated as "negative" are considered to belong to class 0, which encompasses non-fragile subjects. Conversely, the terms designated as "positive" are class 1, which includes fragile subjects. In light of the aforementioned considerations, the following cases can be distinguished:

- A **True Negative (TN)** is a non-fragile subject that has been correctly classified as such.
- A **True Positive (TP)** is a fragile subject that has been correctly classified as such.
- A **False Negative (FN)** is a fragile subject that has been incorrectly classified as non-fragile.
- A **False Positive (FP)** is a non-fragile subject that has been incorrectly classified as fragile.

Table 2.4: Confusion Matrix

True \ Predicted	Negative	Positive
Negative	True Negative	False Positive
Positive	False Negative	True Positive

Accordingly, the metrics employed for performance evaluation, taking into account the previous definitions, are as follows:

- **Accuracy**, defined as the proportion of observations that have been correctly classified as true positives or true negatives

$$Accuracy = \frac{TP + TN}{TP + TN + FP + FN}$$

- **Precision**, which is the ability of the classifier not to label as positive (fragile) a sample that is negative (not fragile)

$$Precision = \frac{TP}{TP + FP}$$

- **Sensitivity**, the ability of the classifier to find all the positive samples, given that frailty is truly present. It indicates the ratio of correctly identified positive instances

$$Sensitivity = \frac{TP}{TP + FN}$$

- **Specificity** is the probability of obtaining a negative classification, given that frailty is really absent;

$$Specificity = \frac{TN}{TN + FP}$$

- **F1-score** is the harmonic mean of precision and sensitivity

$$F1 - score = \frac{2 \cdot TP}{2 \cdot TP + FP + FN}$$

- **Error rate** is the degree of prediction error of a model made with respect to the true model

$$Errore - rate = 1 - Accuracy$$

Chapter 3

Results and Discussion

3.1 Frailty assessment

In collaboration with the University of Turin, the tests and questionnaires utilised for the identification of frailty were evaluated.
The following section presents the values and responses obtained in relation to Fried's phenotype and the TFI questionnaire.
It should be noted that the column labelled "*Hand Grip*" in the Table 3.1 contains the values obtained from the dynamometer test. In this context, the symbols R_i and L_i represent the various acquisitions for the right and left hands, respectively. Furthermore, it is important to highlight that the subject is classified as sedentary based on the PASE score when the value falls below the threshold value of 76 as defined by the WHO.

A general and summary table was generated from the results obtained with both methods of frailty identification. This table included each subject with the relative scores obtained.
It should be noted that for the Fried index, a value greater than three indicates the presence of fragility, while a value between one and two represents a state of pre-fragility. In contrast, for the TFI, the presence of fragility is indicated by a score of five or more.
Upon examination of the values obtained, it becomes evident that none of the subjects exhibited the characteristics of fragility as defined by Fried's index, but rather exhibited pre-fragility. Concurrently, the TFI score indicates that a considerable proportion of the subjects considered fragile did not achieve a value above the threshold. In fact, the majority of them obtained the minimum value required to be classified as fragile. This evidence suggests that, among the subjects analysed in this study, there are no evident cases of frailty under the various points of view analysed.
In order to have more consistent results and distinction between class 0 and class 1, it was decided to consider as belonging to class 1 only those subjects found to be pre-fragile/fragile in both assessment methods namely subjects 2, 3, 4, 11 and 13.

Table 3.1: The data collected through the Fried's Index and the PASE Questionnaire.

Subject	BMI	Height	PASE > 76	Hand Grip						Walk Time	Effort for every action?	Unable to get going?	Recently lost a lot of weight?
				R_1	R_2	R_3	L_1	L_2	L_3				
S1	25.5	1.67	193.8	31.4	30.6	31.2	29.7	32.1	32.1	4.89	0	0	NO
S2	28.9	1.60	110	22.4	21	13.3	12.8	13.6	7.6	4.79	2	2	NO
S3	19.9	1.60	146.7	22.2	22.2	20.7	21.6	21.9	20.7	4.23	2	2	YES
S4	31.2	1.68	111	20	18.9	21	22.5	20.3	23	11.97	0	0	NO
S5	27.9	1.55	173.8	15.9	15.5	15.8	18.7	15.8	16.5	6.89	1	0	NO
S6	23.3	1.63	104.3	40.06	43	38	38.2	40.2	36.5	4.29	1	0	NO
S7	22.8	1.54	74	15.4	16	18	14	13.4	14.8	4.52	2	0	NO
S8	25.7	1.72	217	27.9	28.8	28.6	31.2	31.5	33	4.2	0	0	NO
S9	25.8	1.55	85	23	25.6	17.9	18.7	16.2	16.7	4.77	1	0	NO
S10	37.9	1.78	121	41.6	42.2	39.4	34.4	35.4	34.3	4.79	0	0	NO
S11	30.7	1.50	147.1	11.2	11.6	13.9	10.7	15.8	15.1	5.6	0	0	NO
S12	25.9	1.70	29.3	31.7	31.8	33.2	31.2	30.7	30.5	6.07	0	0	NO
S13	25.9	1.55	78.6	12.6	14.1	12.8	14.5	11.8	14.7	4.59	0	0	NO
S14	22.2	1.63	122.6	25.2	26.4	26.5	26	23.2	23.4	3.8	0	0	NO
S15	24.2	1.70	143.6	42.1	49.1	45.5	34.5	44.3	40.2	3.2	2	2	NO
S16	28.4	1.78	182.9	51.2	51.4	51.3	35.9	44.6	39.5	4.4	0	1	NO
S17	21.5	1.79	96.5	43.5	49.5	52.4	42.6	45.5	43.2	3.72	0	0	NO
S18	22.8	1.65	141.6	25.8	27.7	27.7	14.7	10.6	13.4	3.21	0	0	NO
S19	27.8	1.80	141	30.1	26.7	30.7	29.2	28.2	26.7	4.66	0	0	NO
S20	23	1.68	157.4	17.3	13.5	14.8	25.6	24.5	26.5	4.93	1	0	NO

Table 3.2: Data collected through the TFI, first part.

Subject	Recently lost a lot of weight?	Physically active enough?	Difficulty maintaining walking?	Difficulty balance?	Poor hearing?	Poor eyesight?	Lack of hand strength?	Physical fatigue?
S1	0	0	0	0	0	0	0	0
S2	0	1	1	0	0	0	1	1
S3	1	0	0	0	0	1	1	1
S4	0	0	1	0	1	0	0	0
S5	0	0	0	0	1	1	0	0
S6	0	0	0	0	0	1	0	0
S7	0	0	0	0	0	0	0	1
S8	0	0	0	0	1	1	0	0
S9	0	1	0	0	0	1	1	1
S10	0	1	0	0	0	1	0	0
S11	0	0	0	0	1	1	0	0
S12	0	0	0	0	1	1	0	0
S13	0	0	0	0	0	1	1	0
S14	0	0	0	0	0	1	0	0
S15	0	0	0	0	0	1	0	0
S16	0	0	0	0	0	0	0	0
S17	0	0	0	0	0	0	0	0
S18	0	0	0	0	0	0	1	0
S19	0	1	0	0	0	0	0	0
S20	0	0	0	0	1	0	1	0

Table 3.3: Data collected through the TFI, second part.

Subject	Memory problems?	Feeling down in the last month?	Feeling anxious/nervous in the last month?	Able to cope with problems?	Lives alone?	Feels the lack of people around?	Receives sufficient support?
S1	0	0	1	0	0	1	0
S2	0	1	1	1	0	0	0
S3	0	1	1	1	1	1	0
S4	0	1	0	1	0	1	0
S5	0	1	0	0	1	1	0
S6	0	1	1	0	0	0	0
S7	0	0	1	0	0	0	0
S8	0	0	1	0	1	1	0
S9	0	0	1	0	0	1	0
S10	0	1	0	0	0	0	0
S11	0	1	0	0	1	1	0
S12	0	0	0	0	1	0	0
S13	0	1	0	0	1	1	0
S14	0	1	1	0	0	0	0
S15	0	1	0	0	0	1	0
S16	0	0	1	0	0	0	0
S17	0	1	0	0	0	0	0
S18	0	0	1	0	0	0	0
S19	0	0	0	0	0	0	0
S20	0	0	0	0	1	1	0

Table 3.4: Total results for Fried Index and TFI.

Subject	Age	Total Fried	Total TFI
S1	83	0	2
S2	75	1	7
S3	75	2	9
S4	87	2	5
S5	75	0	5
S6	67	0	3
S7	64	1	2
S8	73	0	5
S9	68	0	6
S10	67	0	3
S11	89	1	5
S12	89	1	3
S13	86	1	5
S14	61	0	3
S15	62	1	3
S16	63	0	1
S17	61	0	1
S18	62	0	2
S19	64	0	1
S20	80	1	4

Pre-fragile

Fragile

3.2 Pre-processing

The diagram of the performance of the hook grip exercise of subject one is presented below as an illustrative example Figure 3.1. Each colour represents a different acquisition channel. It can be inferred that the channels with greater amplitude are those that acquire the muscles most involved in the exercise under examination.
In general, when analysing the various signals obtained, it was noted that many had very

low amplitudes, on the order of tens of μV. This was not observed in specific exercises, indicating that the selection of exercises was appropriate. However, it was noted in some subjects. This may be attributed to the subject's general physical condition and/or their inability to perform certain exercises.

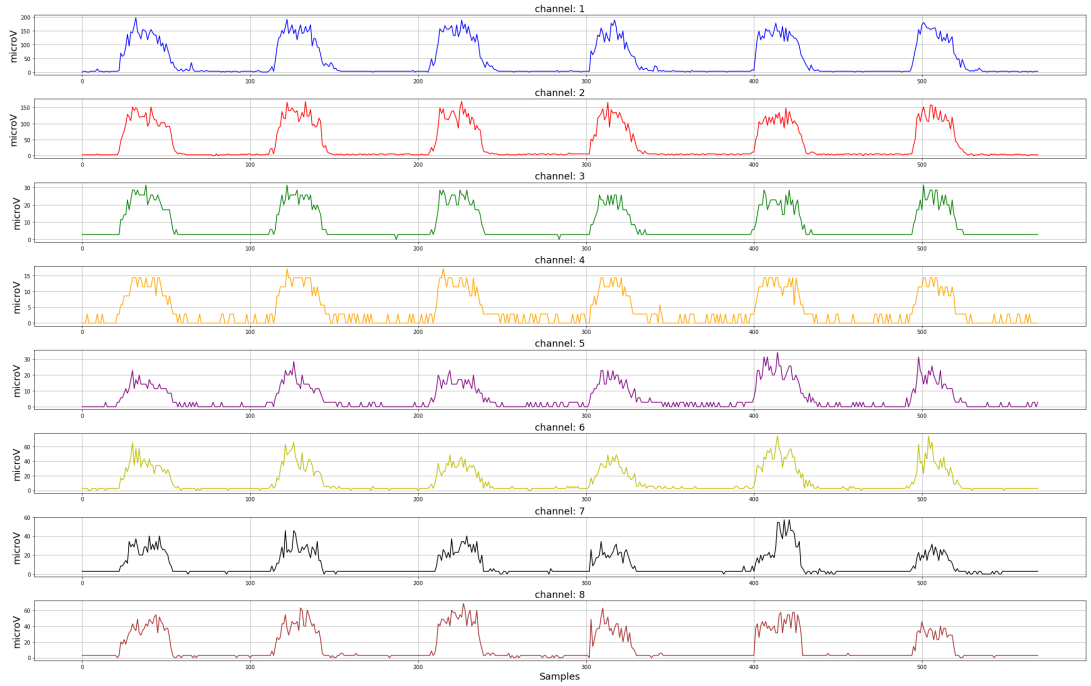

Figure 3.1: The EMG trace of subject 1, right hand exercise, is presented above. The subject was instructed to perform a "Hook grasp" excercise.

Moreover, an examination of the PSD reveals that the signal power is predominantly concentrated at frequencies below 200 Hz. This phenomenon is a common occurrence in EMG signals of voluntary contraction. The frequency of the signal is approximately 150 Hz when decisive movements are performed in a short period of time (approximately 100 ms) [52].
This power distribution justifies the application of a low-pass filter with a cut-off frequency of 200 Hz, adopted in this study for the envelope calculation. In fact, as the signal power is mainly concentrated at frequencies below 200 Hz, the elimination of the higher frequencies reduces noise at higher frequencies.
The result of the low-pass filter used to calculate the envelope is shown below, superimposed on the original signal for each channel. This allows the differences between the signals to be observed. In calculating the envelope, it was decided to preserve the general EMG trace, attempting to maintain the shape as much as possible in order to minimise the loss of information, as well as avoiding to anticipate the on/off instants.
It should be noted that the signal represented in Figure 3.3 has already undergone the normalisation process described in subsection 2.5.4. As the "Hook grasp" exercise is represented here, it is related to the hand movement exercise set. Therefore, the normalisation was carried out using the "Spherical grasp" exercise as a reference.

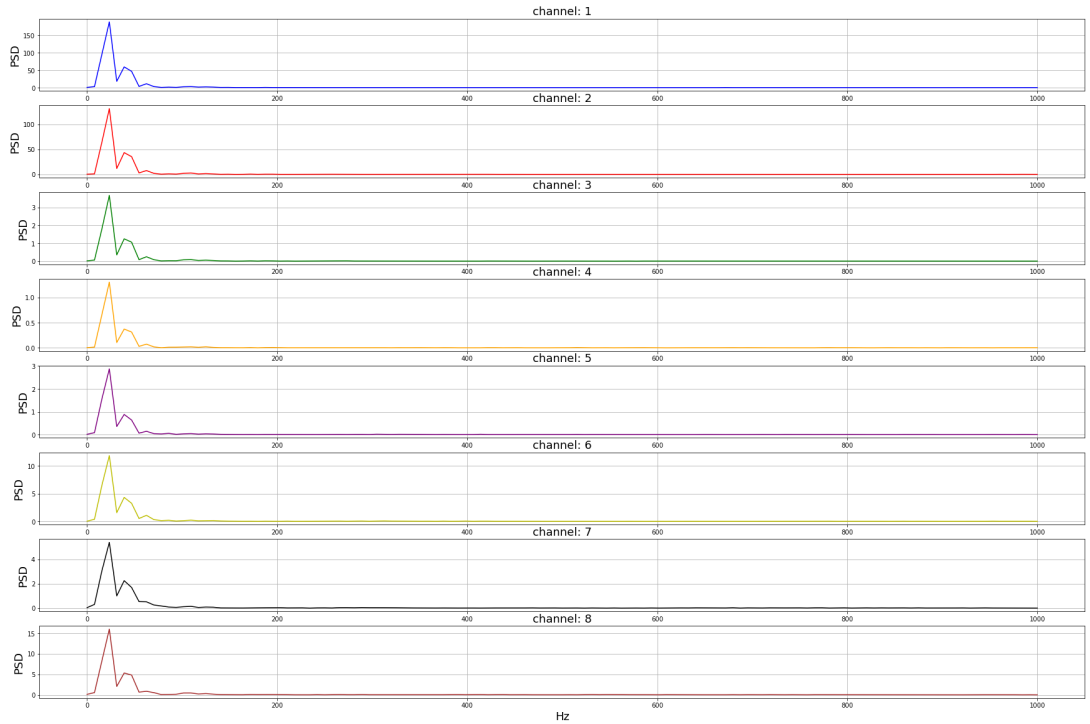

Figure 3.2: PSD of subject 1, right hand "Hook grasp" exercise.

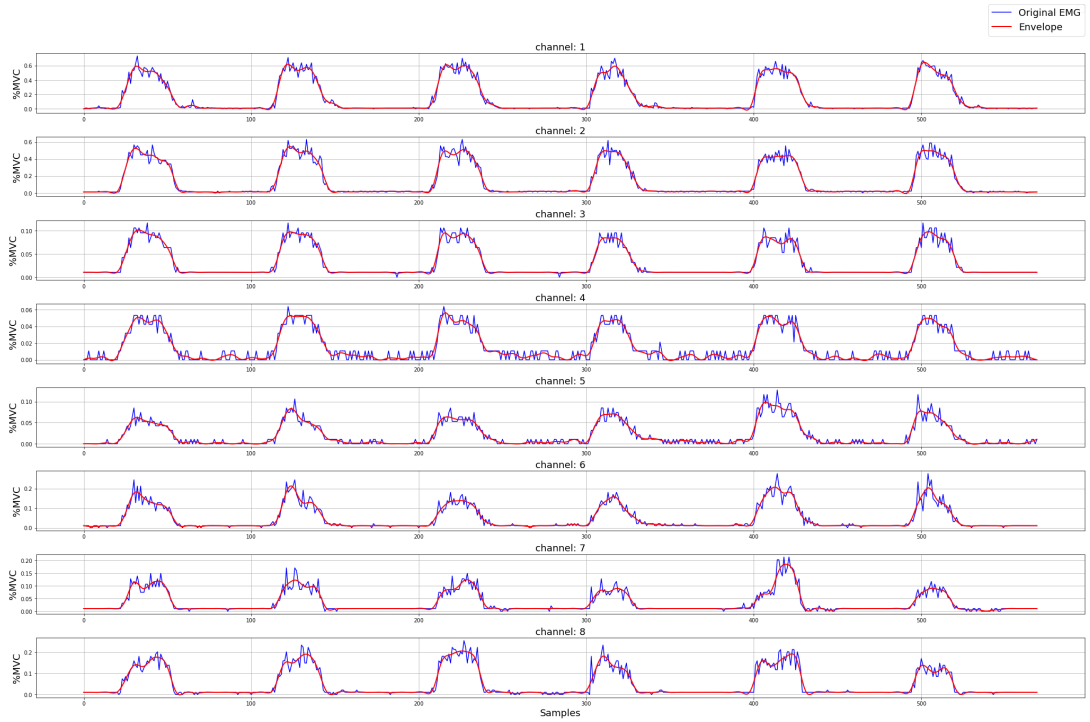

Figure 3.3: EMG signal envelope superimposed on the original signal of subject 1, right hand "Hook grasp" exercise.

3.3 Identification of repetitions and evaluation of SNR

The repetitions were identified by means of a threshold, which is shown in Figure 3.3 with the green dashed line. This threshold allowed the identification of peaks, which are

indicated by the 'x' on the graph, within the various segments under consideration. Of all the peaks identified, the largest was chosen, as this was considered to be the centre of the activation window. The figure below then shows the result.
These repetitions were then used to calculate a threshold for the noise present within the repetition under analysis. This approach allowed for greater precision in calculating the threshold than would have been possible had a general threshold been determined for the entire signal, which included all six repetitions. This resulted in more accurate noise identification, with the SNR values being more satisfactory.

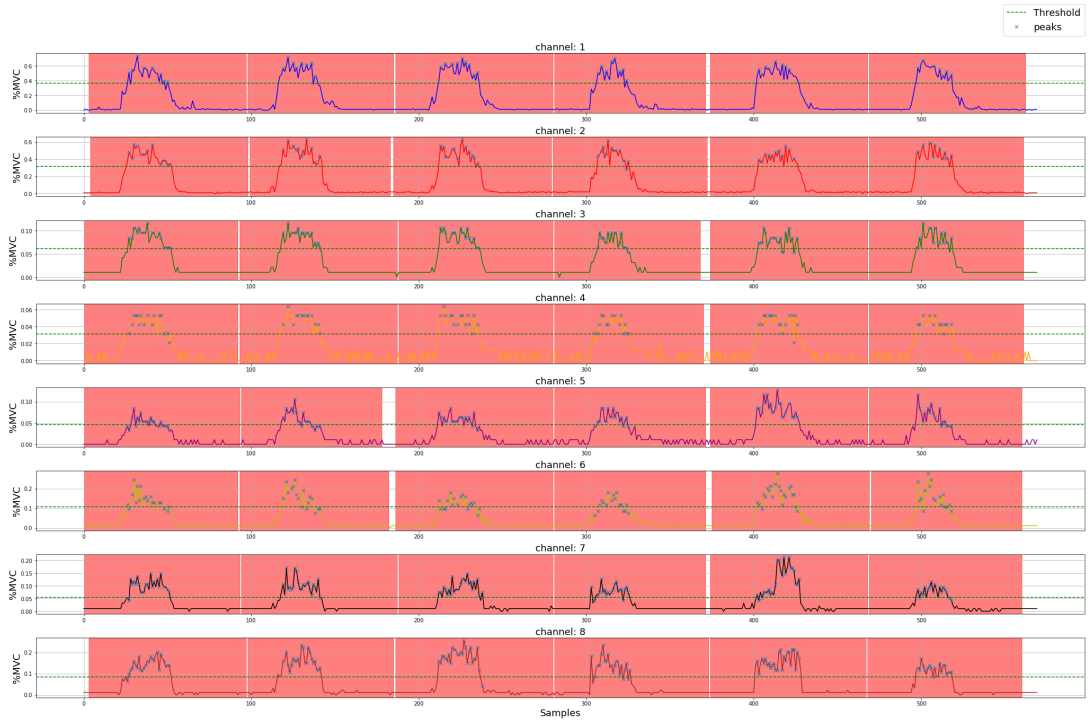

Figure 3.4: Identified repetitions. The threshold, represented by the dashed green line, was employed to identify peaks, indicated by the symbol 'x'. The major was employed as the centre of the activation window, which is highlighted in red. This process was repeated for each repetition of each channel of the various exercises.

The average signal-to-noise ratio (SNR) value was calculated for each acquisition channel of each signal. The average SNR was found to range from 10 dB to approximately 20 dB, indicating that the signals were of fair quality, given that an optimum SNR value of 40 dB is typically considered to be the benchmark for quality.
However, there were some signals whose SNR was less than 8 dB. A significant proportion of these signals belonged to subjects that were defined as fragile, at least by one of the two evaluation methods that were used. This could indicate a reduction in the muscular intensity exhibited by the subjects, which may result in an increase in noise levels. Conversely, incorrect positioning of the device could be a contributing factor. In fact, during the exercise sessions, REMO® may have moved, causing the acquisition electrodes to shift. Another potential source of the noise is the arrangement of the electrodes relative to the forearm muscles. It is important to note that the subjects had different forearm circumferences. While the cuff is stretchable, allowing closure up to 27 cm in circumference, the electrode array is fixed. Consequently, a larger forearm was not fully covered by the acquisition electrodes. This may have resulted in the activity of the muscles being picked up less effectively, particularly during exercises that involved the

posterior forearm muscles.
In certain instances, the signal quality was found to be unsatisfactory in only a few channels, whereas the remainder exhibited a more favourable SNR. This phenomenon may be attributed to the nature of the exercise. In fact, some exercises required the activation of only a subset of the muscles present, which were only picked up by the nearby electrodes. This resulted in poor-quality signals in the channels whose electrodes were further away, as they were only able to acquire noise.
Finally, the variability of signal quality is strongly influenced by the physical characteristics of the subjects. In fact, a subject's skin type and degree of training can significantly impact the electrode-skin contact in the former case, and the intensity of muscular activity in the latter. In the event that the signal is too weak, it is in fact overwhelmed by the effects of artefacts and interference, resulting in a reduction of the signal-to-noise ratio.

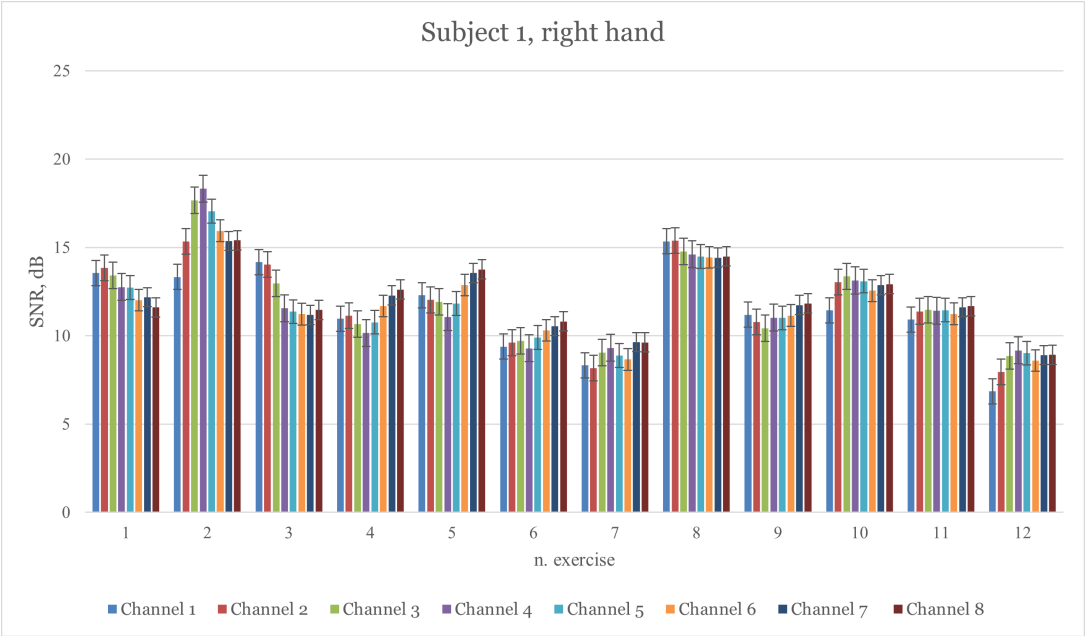

Figure 3.5: Here is the variation of Subject 1's SNR between the different channels and exercises.

3.4 Feature extraction and Statistical test

As previously stated, we opted to calculate the features in two distinct manners to ascertain potential discrepancies in the final outcome. Both methods incorporate an average of the values within the acquisition channel under consideration to mitigate the variability of the various repetitions.
Subsequently, statistical tests were conducted on both datasets to assess whether the feature under investigation exhibited a statistically significant difference between the two classes (Table 3.5).

Feature	Test U p-value	
	Dataset 1	Dataset 2
RMS	0.009471669	0.009354411
VAR	0.100419022	0.384309737
STD	0.121664435	0.384309737
MAV	0.000697667	0.000819895
WL	0.000422332	0.000292813
WAMP	1.46066E-05	0.007437711
IsEMG	0.000148476	7.06187E-05
SSI	0.002564485	0.002077241
Activations	0.023957346	0.009731861
f-Mean	0.864424819	0.056927994
f-Median	1	1
AR2.1	0.00016976	3.77979E-05
AR2.2	0.6802682	0.021392599
AR2.3	0.943709305	0.734991619
AR6.1	0.005635248	0.002083216
AR6.2	0.992147025	0.324366657
AR6.3	0.146748485	0.002845439
AR6.4	2.35378E-05	0.003561043
AR6.5	0.23604123	0.077815855
AR6.6	0.000492802	0.185924017
SSC	0.598133184	4.92693E-07
AAC	0.005262093	0.005402887
KURT	0.75117032	0.292670481
SKEW	0.189941751	0.016154864
CREST	0.959386287	0.157522045
ENTR	0.026850454	0.048279526

Table 3.5: The results of the statistical tests of features are presented below for the two types of dataset. The AR2.i and AR6.i features represent the various obtained values of the autoregressive coefficients. The AR2 coefficients of order 2 have three values, while the AR6 coefficients of order 6 have six values. A p-value of 0.05 was selected as the threshold, indicating that for $p<0.05$ (shown in yellow), the feature exhibits a significant difference between the two classes. Conversely, for $p>0.05$, the feature is deemed to be insignificant.

A comparison of the f-Median values for the two classes (0 and 1) revealed that there was no significant difference. This is consistent with the expected outcome, given the nature of the signal.
The analysis indicated that the most effective features for discriminating fragile and non-fragile subjects lie within the temporal domain. This lends support to the decision to implement these features, as they are simpler and more lightweight computationally.

3.5 Classification

Once the classifier had been implemented, a series of tests were conducted with the objective of comparing its performance.
In particular, the performance of the classifier was evaluated for each dataset by training the classifier using normalised signals without and with envelope. Furthermore, the efficacy of PCA was evaluated for both configurations.
It is important to note that within the cross-validation algorithm for each dataset, the optimal parameters for kernel variation were identified through the use of computational time and average accuracy as evaluation metrics. In order to train the classifier, the kernel was selected with the appropriate parameters that achieved a reasonable balance between time and performance. From the outset of the tests, the classifiers with kernel = polynomial exhibited considerable computational times of the order of 10,000 seconds. This observation led to the decision to exclude this kernel from the subsequent analysis.

The results of the various tests are presented below.

3.5.1 Feature Dataset 1 with envelope

Kernel Test	C	gamma	n_comp	Accuracy	Time (s)
linear	0.1	0.001	18	69.35	10.4
rbf	10	0.1	15	76.05	3.5
sigmoid	100	0.01	15	75.53	3.5

Table 3.6: Results of cross-validation for kernels and parameter for Dataset 1 with envelope.

Given the considerable similarity in the performance of the kernel=RBF and kernel = sigmoid models, tests were conducted using both.

	Kernel	C	Gamma	n_comp	Accuracy %	F1-score %	Precision %	Sensitivity %	Specificity %
Test 1 with PCA	rbf	10	0.1	15	59.57	31.08	22.05	52.63	61.02
Test 2 without PCA	rbf	10	0.1	15	60.18	30.68	21.96	50.87	62.13
Test 3 with PCA	sigmoid	100	0.01	15	58.96	37.78	25.62	71.92	56.25
Test 4 without PCA	sigmoid	100	0.01	15	64.74	40.81	28.77	70.17	63.60

Table 3.7: Comparison of different kernel tests with and without PCA for Dataset 1 with envelope.

It can be observed that the performance is suboptimal. In order to facilitate a comparative analysis of the various methods, the model highlighted in yellow was identified as the most effective, employing a sigmoid kernel without the use of PCA.

3.5.2 Feature Dataset 1 without envelope

Kernel Test	C	gamma	n_comp	Accuracy	Time (s)
linear	1	0.001	18	76	8.3
rbf	100	0.1	18	72.08	3.6
sigmoid	10	0.01	18	77.47	3.4

Table 3.8: Results of cross-validation for kernels and parameter for Dataset 1 without envelope.

In this instance, the cross-validation results indicate comparable average accuracies and processing times, which is why we proceeded to attempt training the model in all configurations.

	Kernel	C	Gamma	n_comp	Accuracy %	F1-score %	Precision %	Sensitivity %	Specificity %
Test 1 with PCA	linear	1	0.001	18	61.39	39.23	26.97	71.92	59.19
Test 2 without PCA	linear	1	0.001	18	60.79	38.27	26.31	70.17	58.82
Test 3 with PCA	rbf	100	0.1	18	57.77	38.22	25.59	75.43	54.04
Test 4 without PCA	rbf	100	0.1	18	58.35	38.00	25.60	73.68	55.14
Test 5 with PCA	sigmoid	10	0.01	18	58.05	36.11	24.52	68.42	55.88
Test 6 without PCA	sigmoid	10	0.01	18	59.57	35.12	24.32	63.15	58.82

Table 3.9: Comparison of different kernel tests with and without PCA for Dataset 1 without envelope.

Nevertheless, it can be observed that the performance is slightly inferior to that observed in the previous case. In particular, it can be observed that the sensitivity is high, indicating a robust capacity to correctly classify class 1. Conversely, however, the specificity is slightly greater than 50 %, which indicates that class 0 is not particularly recognised. Consequently, these models tend to classify subjects as frail when they are not, which results in a high sensitivity. Although this may appear to be a rather conservative approach, it does indicate a limited ability to distinguish between classes 0 and 1. This hypothesis is also corroborated by the low accuracy.

3.5.3 Feature Dataset 2 with envelope

Kernel Test	C	gamma	n_comp	Accuracy	Time (s)
linear	10	0.001	8	67.20	8.3
rbf	1	0.1	3	68.59	3.6
sigmoid	0.1	10	12	66.44	3.6

Table 3.10: Results of cross-validation for kernels and parameter for Dataset 2 with envelope.

The radial basis function and sigmoid kernels were employed in the training of the model, resulting in the following performance metrics.

	Kernel	C	Gamma	n_comp	Accuracy %	F1-score %	Precision %	Sensitivity %	Specificity %
Test 1 with PCA	rbf	1	0.1	3	64.43	36.06	26.19	57.89	65.80
Test 2 without PCA	rbf	1	0.1	3	57.75	36.52	24.69	70.17	55.14
Test 3 with PCA	sigmoid	0.1	10	12	58.05	34.90	23.80	75.90	56.60
Test 4 without PCA	sigmoid	0.2	10	12	59.57	34.48	23.97	61.59	59.19

Table 3.11: Comparison of different kernel tests with and without PCA for Dataset 2 with envelope.

As Table 3.9, it can be observed that the sensitivity is high, despite the specificity. It does indicate a limited ability to distinguish between classes 0 and 1. This hypothesis is also highlighted by the low accuracy.
Hence, once more, the performance remains unsatisfactory, which is the reason why they were rejected.

3.5.4 Feature Dataset 2 without envelope

Kernel Test	C	gamma	n_comp	Accuracy	Time (s)
linear	100	0.001	18	65.65	11.7
rbf	1	0.1	5	68.90	3.7
sigmoid	0.1	10	3	74.46	3.3

Table 3.12: Results of cross-validation for kernels and parameter for Dataset 2 without envelope.

In the training of the model, the RBF and sigmoid kernels were employed. The following performances were then obtained:

	Kernel	C	Gamma	n_comp	Accuracy %	F1-score %	Precision %	Sensitivity %	Specificity %
Test 1 with PCA	rbf	1	0.1	5	67.47	41.53	30.15	66.66	67.64
Test 2 without PCA	rbf	2	0.1	6	69.60	43.18	31.93	66.66	70.22
Test 3 with PCA	sigmoid	0.1	10	3	59.57	33.16	23.23	59.90	40.42
Test 4 without PCA	sigmoid	0.2	10	3	59.58	33.17	23.23	59.90	40.42

Table 3.13: Comparison of different kernel tests with and without PCA for Dataset 2 without envelope.

In this instance, the model exhibiting the most optimal performance was generated through the use of the RBF kernel, particularly in the absence of principal component analysis (PCA).

At this juncture, tests were conducted on the statistically significant features for the respective datasets, as reported in Table 3.5.

3.5.5 Feature Dataset 1 with envelope - statistically significant

Kernel Test	C	gamma	n_comp	Accuracy	Time (s)
linear	0.1	0.001 66	5	68.20	3.6
rbf	10	0.1	12	72.89	2.3
sigmoid	100	0.01	12	74.39	2.2

Table 3.14: Results of cross-validation for kernels and parameter for Feature Dataset 1 with envelope - statistically significant.

	Kernel	C	Gamma	n_comp	Accuracy %	F1-score %	Precision %	Sensitivity %	Specificity %
Test 1 with PCA	rbf	10	0.1	12	63.22	37.30	26.47	63.15	63.23
Test 2 without PCA	rbf	10	0.1	12	63.52	37.50	26.66	63.15	63.60
Test 3 with PCA	sigmoid	100	0.01	12	67.17	37.93	28.20	57.89	69.11
Test 4 without PCA	sigmoid	100	0.01	12	66.26	37.28	27.50	57.89	68.00

Table 3.15: Comparison of different kernel tests with and without PCA for Feature Dataset 1 with envelope - statistically significant.

The results demonstrate that the models trained using the RBF kernel yield balanced outcomes between the two classes, both with and without the application of PCA. Consequently, in order to achieve the same level of performance, we have elected to consider Test 2, which will result in a reduction in computational costs and an easier training process in the absence of PCA.

3.5.6 Feature Dataset 1 without envelope - statistically significant

Kernel Test	C	gamma	n_comp	Accuracy	Time (s)
linear	0.1	0.001	12	55.43	3.2
rbf	100	10	3	64.89	2.3
sigmoid	100	0.01	12	65.33	2.3

Table 3.16: Results of cross-validation for kernels and parameter for Feature Dataset 1 without envelope - statistically significant.

	Kernel	C	Gamma	n_comp	Accuracy %	F1-score %	Precision %	Sensitivity %	Specificity %
Test 1 with PCA	rbf	100	10	3	53.19	22.99	16.08	40.35	55.88
Test 2 without PCA	rbf	100	10	3	68.69	11.96	11.66	12.80	80.51
Test 3 with PCA	sigmoid	100	0.01	12	66.26	36.57	27.11	56.14	68.38
Test 4 without PCA	sigmoid	100	0.01	12	67.17	37.20	27.82	56.14	69.48

Table 3.17: Comparison of different kernel tests with and without PCA for Feature Dataset 1 without envelope - statistically significant.

As evidenced by the performance metrics, while the accuracy of these models is comparable to that of the previously selected models, they exhibit significantly lower sensitivity rates, resulting in a high prevalence of false negatives. This indicates that these models are capable of accurately classifying class 0, thereby enhancing overall accuracy. However, they are less effective in classifying class 1. Consequently, such models lack discriminatory power.

3.5.7 Feature Dataset 2 with envelope - statistically significant

Kernel Test	C	gamma	n_comp	Accuracy	Time (s)
linear	1	0.001	12	70.00	34.6
rbf	1	0.01	8	80.64	2.3
sigmoid	0.1	10	12	71.04	2.2

Table 3.18: Results of cross-validation for kernels and parameter for Feature Dataset 2 with envelope - statistically significant.

	Kernel	C	Gamma	n_comp	Accuracy %	F1-score %	Precision %	Sensitivity %	Specificity %
Test 1 with PCA	linear	1	0.001	12	62.91	40.19	27.89	71.92	61.02
Test 2 without PCA	linear	1	0.001	12	63.52	40.59	28.27	71.92	61.76
Test 3 with PCA	rbf	1	0.01	8	64.74	39.58	28.14	66.66	64.33
Test 4 without PCA	rbf	1	0.01	8	63.52	40.00	27.97	70.17	62.13
Test 5 with PCA	sigmoid	0.1	10	12	57.77	34.74	23.71	64.91	56.25
Test 6 without PCA	sigmoid	0.1	10	12	58.05	34.28	23.52	63.15	56.98

Table 3.19: Comparison of different kernel tests with and without PCA for Feature Dataset 2 with envelope - statistically significant.

The highlighted model exhibits lower accuracy than those previously considered, yet it displays balanced sensitivity and specificity values. This indicates that the model is capable of distinguishing between the two classes in a discrete manner, without exhibiting a bias towards either.

3.5.8 Feature Dataset 2 without envelope - statistically significant

Kernel Test	C	gamma	n_comp	Accuracy	Time (s)
linear	0.01	0.001	12	68.33	4.2
rbf	10	0.1	12	69.51	2.3
sigmoid	1	1	5	72.66	2.2

Table 3.20: Results of cross-validation for kernels and parameter for Feature Dataset 2 without envelope - statistically significant.

	Kernel	C	Gamma	n_comp	Accuracy %	F1-score %	Precision %	Sensitivity %	Specificity %
Test 1 with PCA	rbf	10	0.1	12	58.66	38.18	25.75	73.68	55.51
Test 2 without PCA	rbf	10	0.1	12	58.66	38.70	26.06	75.43	55.14
Test 3 with PCA	sigmoid	1	1	5	56.38	31.70	21.85	57.89	56.61
Test 4 without PCA	sigmoid	1	1	5	45.59	23.17	15.34	47.36	45.22

Table 3.21: Comparison of different kernel tests with and without PCA for Feature Dataset 2 without envelope - statistically significant.

The models illustrated above demonstrate suboptimal performance. Test 4, in particular, exhibits an accuracy of less than 50 %, which indicates a tendency to misclassify subjects. In general, all models exhibit low specificity, indicating a difficulty in recognizing non-fragile subjects. Consequently, all of the aforementioned models were rejected.

It is evident that the utilisation of PCA does not enhance the models, and in some instances, it may even result in a decline in performance. One possible explanation is that PCA reduces the dimensionality of the data by projecting them onto a new space with fewer dimensions, while maintaining the maximum variance. Nevertheless, the maximum variance does not always correspond to the most pertinent features for classification. It is possible that PCA is eliminating some components that, although having a smaller variance, are crucial for distinguishing between frail and non-frail subjects. Moreover, it is a linear technique that is most effective when the data are linearly distributed. Nevertheless, sEMG signals frequently exhibit a complex, non-linear structure. In such instances, PCA may be unable to identify the requisite features for effective classification.

Another potential reason for this discrepancy could be the selection of the number of components. In fact, although this was selected within the cross-validation algorithm, a considerable number of models had a very low number of components (3 or 5), which could result in a significant loss of information. Conversely, models with a large number of components (18) may have been susceptible to the risk of maintaining noise.

3.5.9 Model comparison

The following section presents a more straightforward comparison of the models selected above.

	Kernel	C	Gamma	PCA, n_comp	Accuracy %	F1-score %	Precision %	Sensitivity %	Specificity %
Dataset 1 with envelope	sigmoid	100	0.01	no	64.74	40.81	28.77	70.17	63.60
Dataset 2 without envelope	rbf	2	0.2	6	69.60	43.18	31.93	66.66	70.22
Dataset 1 with envelope statistically significant	rbf	10	0.1	12	63.22	37.30	26.47	63.15	63.23
Dataset 1 with envelope statistically significant	rbf	10	0.1	12	63.52	37.50	26.66	63.15	63.60
Dataset 2 with envelope statistically significant	rbf	1	0.01	8	64.74	39.58	28.14	66.66	64.33

Table 3.22: Comparison of different model's performance.

In order to facilitate a more accurate understanding of the proportion of correctly and incorrectly classified data, the confusion matrices are presented below.

		Predicted Class	
		Negative	**Positive**
Actual Class	**Negative**	63.6 %	36.4 %
	Positive	29.8 %	70.2 %

Table 3.23: Confusion Matrix of Dataset 1 with envelope

		Predicted Class	
		Negative	**Positive**
Actual Class	**Negative**	70.2 %	28.8 %
	Positive	33.3 %	66.7 %

Table 3.24: Confusion Matrix of Dataset 2 without envelope

		Predicted Class	
		Negative	**Positive**
Actual Class	**Negative**	63.2 %	36.7 %
	Positive	36.8 %	63.1 %

Table 3.25: Confusion Matrix of Dataset 1 with envelope with PCA- statistically significant

		Predicted Class	
		Negative	**Positive**
Actual Class	**Negative**	63.6 %	36.4 %
	Positive	36.8 %	63.1 %

Table 3.26: Confusion Matrix of Dataset 1 with envelope without PCA - statistically significant

		Predicted Class	
		Negative	**Positive**
Actual Class	**Negative**	64.3 %	35.5 %
	Positive	33.3 %	66.7 %

Table 3.27: Confusion Matrix of Dataset 2 with envelope - statistically significant

Among the CMs, it can be observed that Table 3.24 has the highest percentage of correct classification, with a clear preference for the correct classification of class 0 over 1. Furthermore, it exhibits a slightly higher percentage of false negatives than false positives. In principle, in order to be more conservative, it would be preferable to have a greater number of FPs than FNs. This is because it would be preferable to identify a potential frailty and conduct further analysis that may subsequently invalidate the algorithm, rather than having the possibility of failing to recognise a fragility where one is present.
Table 3.25 and Table 3.26 demonstrate that the two models exhibit essentially identical performance characteristics, as they originate from the same configuration of the underlying data set. Nevertheless, among the selected models, they are the ones with the lowest correct classified, although the difference is marginal. It is therefore necessary to exclude them from further consideration.
In contrast to the aforementioned models, the Table 3.27 is also excluded. Indeed, this model exhibits a lower F1-score and precision value than the former CMs.
Consequently, the first two models are the most effective of those analysed. The first model exhibits a slightly inferior performance compared to the second, yet it demonstrates a higher sensitivity. This indicates that it is more adept at identifying vulnerable subjects, including the identification of errors and an increased percentage of false positives, which results in a more cautious approach than the second model under analysis.
Furthermore, it is evident that the datasets comprising only those features deemed statistically significant exhibited a slight decline in performance when evaluated using the F1-score. It is possible that this discrepancy is attributable to the statistical tests evaluating individual features, whereas the combination of features might have carried additional information. However, it can be observed that these models exhibit balanced recognition of the two classes, with comparable sensitivity and specificity values. In contrast, the SVM demonstrated a preferential recognition of a specific class when utilising the complete datasets.
Concerning the two dataset configurations (Feature Dataset 1 and Feature Dataset 2) did not result in any discernible differences. Conversely, the use of the envelope led to a general improvement in performance, with the exception of one specific case (Table 3.13).

In general, it is evident that the performance is not optimal. This may be attributed to a multitude of potential causes. Firstly, it is observed that the number of subjects considered to be fragile was considerably lower than the number of subjects classified as

non-fragile. This resulted in an imbalanced dataset, which made it more challenging to train the classifier with limited data.
It was also observed that the subjects analysed in this study were predominantly healthy individuals with an active social life and minimal sedentary behaviour. As a result, the identification of frailty, as evidenced by Table 3.4, was not entirely evident. In this study, there were no cases of frailty that were particularly obvious. In fact, the scores obtained indicated cases of pre-frailty with regard to Fried's index and low fragility scores with respect to TFI. Therefore, the differentiation between the two categories was considerably more challenging and intricate.
Furthermore, it is highlighted that the quality of the signals was not particularly optimal. This would have had a particularly detrimental impact on the performance of the model. In fact, the calculation of features on signals with a low signal-to-noise ratio leads to a measurement that is significantly affected by noise, with the greatest impact observed at the lowest SNR.

Chapter 4

Conclusion

The objective of this research was to develop an automated method for the identification of frailty, with the aim of enhancing the efficiency and reliability of existing techniques. This study was conducted using a wireless device designed to remotely rehabilitate the forearm of post-stroke patients, REMO® by Morecognition s.r.l., which consists of a flexible array of eight electrodes.
In collaboration with the University of Turin, a protocol of exercises concerning hand and wrist movements was devised to activate the muscles of interest, namely the ulnar flexor of the carpus, radial flexor of the carpus, radial extensor of the carpus and ulnar extensor of the carpus. A total of 20 subjects, with an average age of 77.05 $\pm$ 11.09 years, were recruited for this protocol. The signals were taken from both upper limbs.
The signals obtained from the armband had already undergone filtration, rectification and smoothing, with the RMS value calculated over 64 ms windows. This was corroborated by means of power spectral density analysis. This also permitted the selection of an appropriate threshold for the envelope calculation, which was conducted subsequent to the normalisation of the signals themselves. As no signals from exercises specifically designed for MVC calculation were acquired, two exercises, one for hand movements and one for wrist movements, were chosen as references for normalisation. In particular, the exercises "Repeated dorsiflexion/volar flexion with elbow at 90°" for the wrist and "Spherical grasp" for the hand were selected for analysis because they are commonly referenced in literature and because they were observed in every subject. In fact, due to connectivity and storage issues with the acquisition device, some subjects presented missing exercises.
Two widely used and studied frailty determination methods were employed: The Fried's Index and the TFI questionnaire were utilised, with additional questions from the PASE scale employed to assess sedentary behaviour and questions from the CES-D Scale applied to quantify energy loss. The combined assessments identified five subjects with a mild frailty status, as determined by both methodologies.
Once a class was associated with all the subjects, the automatic classifier was implemented by calculating the features most commonly used in the literature. The decision was taken to utilise an support vector machine (SVM) classifier, given its prevalence in the literature in the context of pattern recognition. A KNN (K-nearest neighbors) classifier was also implemented, however its performance was significantly inferior to the SVM, and as a consequence, it was excluded from the results comparison. Furthermore, the use of principal component analysis (PCA) was implemented within the SVM training pipeline to perform dimensionality reduction. This approach did not result in an improvement in performance, likely because maintaining maximum variance does not correspond with

the optimal features for classification. Additionally, the choice of the optimal number of components is crucial for a complete representation of information.
In the performance evaluation, sensitivity and specificity were assessed to highlight the ability of the various models to correctly classify one of the two classes. In particular, the sensitivity was found to be greater than 65 % and the specificity was found to be 70 %, indicating that the model has a fair ability to recognise frailty.
It can be observed that the performance in question is not optimal. This may be attributed to a number of potential causes. One of the principal factors is the limited number of subjects within the dataset who could be considered fragile. This resulted in difficulties during the training of the classifier, as an attempt was made to create a balanced training set, which in turn limited the samples on which the SVM was trained. Moreover, it is stressed that the subjects considered fragile exhibited a state of pre-fragility according to Fried's Index and reached the minimum threshold to be considered fragile for the TFI questionnaire. This undoubtedly presented a challenge in the gathering of crucial data on frailty during the feature calculation. Furthermore, the suboptimal signal quality, as indicated by the average SNR values, also affected the implementation of the features, which could therefore have been greatly affected by noise. The poor signal quality may be attributable to the nature of the exercises themselves. Indeed, some exercises necessitated the recruitment of specific muscles, which resulted in the acquisition channels being positioned away from them, thereby allowing noise or the activity of underlying muscles to interfere with the signal, adversely affecting the performance of the classifier.

In essence, however, the value of performance allows for a degree of flexibility within a work such as this, which may be considered a pilot study, aimed at analysing the feasibility of the idea under consideration. In fact, even if superior performance were achieved, the application of the model in real-world settings and on a larger scale would result in a significant decline in performance. This is a common problem in various fields of research due to the great variability present.
Finally, it is important to acknowledge the inherent complexity of the concept of frailty. As previously stated in the chapter 1, it is challenging to grasp the multifaceted nature of this concept. Consequently, the ability to identify it solely through physical activity, as outlined in this study, is a rather complex endeavour.

4.0.1 Future developments

In order to enhance the feasibility of this concept and to facilitate its utilisation in a clinical setting, it may be beneficial to consider the potential for extending the acquisition of sEMG signals to other body districts. One possible avenue for exploration could be the development of an exercise protocol for the acquisition of signals from the lower limbs. Indeed, the lower limbs present a more intense muscular activity in comparison to the upper limbs, which may facilitate the observation of differences in the intensity and shape of the sEMG.
However, this would necessitate the utilisation of wireless wearable devices, such as those employed in the aforementioned study, with a greater number of acquisition channels, or the utilisation of electromyographs with wireless acquisition electrodes that can be applied to precise areas of the limb, in order to have a targeted sampling.
In order to process the data, it would also be appropriate to acquire exercises suitable for measuring the maximal so as to be able to normalise the signals as best as possible and be able to compare them between the various subjects.

Finally, the implementation of features in the frequency domain or the wavelet transform may also be able to capture significant information. Similarly, a cross-validation analysis, such as leave-one-out, may result in stable outcomes and account for potential relationships between features.

Bibliography

[1] Brucoli M., Boffano P., and Benech A. «Fragilità e anziani». In: *La fragilità del paziente oncologico nel distretto testa-collo.* Quaderni Monografici di Aggiornamento AOOI., 2020 (cit. on p. 1).

[2] Lee H, Lee E, and Jang IY. «Frailty and Comprehensive Geriatric Assessment». In: *J Korean Med Sci* (2020) (cit. on p. 1).

[3] Gobbens RJJ, van Assen MALM, Augustijn H, Goumans M, and van der Ploeg T. «Prediction of Mortality by the Tilburg Frailty Indicator (TFI)». In: *J Am Med Dir Assoc.* (2021) (cit. on pp. 1, 3).

[4] Cavazza G and Malvi C. *La fragilità degli anziani. Strategie, progetti, strumenti per invecchiare bene.* Santarcangelo di Romagna: Maggioli Editore, 2014 (cit. on p. 1).

[5] Fried LP, Tangen CM, and Walston J. «Frailty in older adults: evidence for a phenotype». In: *J Gerontol A Biol Sci Med Sci* (2001) (cit. on pp. 1, 2).

[6] Dent E, Kowal P, and Hoogendijk EO. «Frailty measurement in research and clinical practice: A review». In: *Eur J Intern Med.* (2016) (cit. on p. 2).

[7] Rockwood K and Mitnitski A. «Frailty in Relation to the Accumulation of Deficits». In: *Journal of Gerontology* (2007) (cit. on p. 2).

[8] Rockwood K, Fox RA, Stolee P, Robertson D, and Beattie BL. «Frailty in elderly people: an evolving concept». In: (1994) (cit. on p. 2).

[9] Rockwood K, Song X, MacKnight C, Bergman H, Hogan DB, McDowell I, and Mitnitski A. «A global clinical measure of fitness and frailty in elderly people». In: *Canadian Medical Association Journal* (2005) (cit. on p. 2).

[10] Gobbens R. J., Luijkx K. G., Wijnen-Sponselee M. T., and Schols J. M. «Towards an integral conceptual model of frailty». In: *J Nutr Health Aging* (2010b) (cit. on p. 2).

[11] Fried LP, Ferrucci L, Darer J, Williamson JD, and Anderson G. «Untangling the concepts of disability, frailty, and comorbidity: implications for improved targeting and care». In: *J Gerontol A Biol Sci Med Sci* (2004) (cit. on p. 2).

[12] Abellan van Kan A., Rolland Y., Bergman H., Morley J. E., Kritchevsky S. B., and Vellas B. «The I.A.N.A Task Force on frailty assessment of older people in clinical practice». In: *J Nutr Health Aging* (2008) (cit. on p. 2).

[13] Mulasso A, Roppolo M, Gobbens RJ, and Rabaglietti E. «The Italian Version of the Tilburg Frailty Indicator: Analysis of Psychometric Properties.» In: *Res Aging.* (2016) (cit. on p. 3).

[14] Pisani P., Battista M., Nestola D., and Colombo A. «L'utilizzo di indici nella valutazione della fragilità». In: *La fragilità del paziente oncologico nel distretto testa-collo*. Quaderni Monografici di Aggiornamento AOOI., 2020 (cit. on p. 3).

[15] Gobbens RJ, van Assen MA, and Luijkx KG adn Schols JM. «The predictive validity of the Tilburg Frailty Indicator: disability, health care utilization, and quality of life in a population at risk.» In: *Gerontologist* (2012) (cit. on p. 3).

[16] Silan M. *Identificazione dei soggetti fragili nell'ULSS 15: una nuova proposta basata sugli ordinamenti parziali*. 2014/2015 (cit. on p. 3).

[17] D.U. Silverthorn, W.C. Ober, C.E. Ober, and A. Impagliazzo. *Human Physiology: An Integrated Approach*. Pearson Education, Incorporated, 2019 (cit. on pp. 4–6).

[18] Gordon Betts J. et al. «Anatomy and Physiology». In: OpenStax, 2013. Chap. 10.2 Skeletal Muscle. URL: `https://openstax.org/books/anatomy-and-physiology/pages/10-2-skeletal-muscle` (cit. on p. 4).

[19] Widmaier Eric P, Raff Hershel, and Strang Kevin T. *Vander-Fisiologia, seconda edizione*. Casa Editrice Ambrosiana, 2018 (cit. on p. 5).

[20] Winter D.A. *Biomechanics and Motor Control of Human Movement*. John Wiley and Sons New York, 1990 (cit. on p. 6).

[21] P. Konrad. *The ABC of EMG - A Practical Introduction to Kinesiological Electromyography*. Noraxon U.S.A, Inc., Version 1.4 March 2006 (cit. on pp. 6, 7, 9–11).

[22] Basmajian J.V. and De Luca C.J. *Muscles Alive. Their Function Revealed by Electromyography*. Williams Wilkins, 1985 (cit. on p. 6).

[23] Muhammad Zahak Jamal. «Signal Acquisition Using Surface EMG and Circuit Design Considerations for Robotic Prosthesis». In: *Computational Intelligence in Electromyography Analysis*. Ed. by Ganesh R. Naik. Rijeka: IntechOpen, 2012. Chap. 18 (cit. on pp. 8, 9).

[24] Merletti R. *Standards for Reporting EMG Data*. Journal of Electromyography and Kinesiology, 1999 (cit. on pp. 9, 10).

[25] Pascucci G. *L'Eelettromiografia: principio di funzionamento e applicazioni in ambito sportivo*. 2016 (cit. on p. 10).

[26] Morecognition. *Remo Manuale d'uso e manutenzione*. Available at `https://www.morecognition.com/wp-content/uploads/2023/09/Remo_Manuale-duso-e-manutenzione.pdf` (cit. on pp. 13, 14).

[27] Pregnolato G, Rimini D, Baldan F, Maistrello L, Salvalaggio S, Celadon N, Ariano P, Pirri CF, and Turolla A. «Clinical Features to Predict the Use of a sEMG Wearable Device (REMO®) for Hand Motor Training of Stroke Patients: A Cross-Sectional Cohort Study.» In: *Int J Environ Res Public Health.* (2023) (cit. on p. 13).

[28] Hermens H.J., Freriks B., Disselhorst-Klug C., and Rau G. «Development of recommendations for SEMG sensors and sensor placement procedures». In: *Journal of Electromyography and Kinesiology* 10.5 (2000) (cit. on p. 13).

[29] Di Girolamo M., Celadon N., Appendino S., Turolla A., and Ariano P. «EMG-based biofeedback system for motor rehabilitation: a pilot study». In: *IEEE Biomedical Circuits and Systems Conference (BioCAS)*. 2017 (cit. on p. 13).

[30] Rimini D. et al. «sEMG-biofeedback armband for hand motor rehabilitation in stroke patients: a preliminary pilot longitudinal study». In: *2020 IEEE International Symposium on Medical Measurements and Applications (MeMeA)*. 2020, pp. 1–5 (cit. on p. 13).

[31] Gladstone D.J., Danells C.J., and Black S. E. «The Fugl-Meyer Assessment of Motor Recovery after Stroke: A Critical Review of Its Measurement Properties». In: *Neurorehabilitation and Neural Repair* (2002) (cit. on p. 14).

[32] Fugl-Meyer AR, Jaasko L, Leyman I, Olsson S, and Steglind S. «The post-stroke hemiplegic patient. A method for evaluation of physical performance.» In: *Scand J Rehabil Med* (1975) (cit. on p. 15).

[33] Washburn R.A., McAuley E.a nd Katula J., Mihalko S.L., and Boileau R.A. «The Physical Activity Scale for the Elderly (PASE): evidence for validity». In: *Journal of Clinical Epidemiology* (1999) (cit. on p. 16).

[34] Radloff L.S. «The CES-D Scale: a self-report depression scale for research in the general population.» In: *Applied Psychological Measurement* (1977) (cit. on p. 16).

[35] Naik G.R. «Computational intelligence in electromyography analysis: a perspective on current applications and future challenges». In: 2012. Chap. 7 (cit. on p. 17).

[36] Dahlqvist C., Enquist H., Löfqvist L., and Nordander C. «The effect of two types of maximal voluntary contraction and two electrode positions in field recordings of forearm extensor muscle activity during hotel room cleaning.» In: *Int J Occup Saf Ergon* (2019) (cit. on p. 18).

[37] Turgunov A., Zohirov K., Ganiyev A., and Sharopova B. «Defining the Features of EMG Signals on the Forearm of the Hand Using SVM, RF, k-NN Classification Algorithms». In: *2020 Information Communication Technologies Conference (ICTC)*. 2020 (cit. on pp. 20, 22, 23).

[38] Andrade A.O. and Andrade C.I. «On the relationship between features extracted from EMG and force for constant and dynamic protocols.» In: *Annu Int Conf IEEE Eng Med Biol Soc.* (2012) (cit. on pp. 20, 22–24).

[39] Al Omari F., Hui J., Mei C, and Liu G. «Pattern Recognition of Eight Hand Motions Using Feature Extraction of Forearm EMG Signal.» In: *Proc. Natl. Acad. Sci., India, Sect. A Phys. Sci.* (2014) (cit. on pp. 20, 22, 23).

[40] Oskoei M.A. and Hu H. «Support Vector Machine-Based Classification Scheme for Myoelectric Control Applied to Upper Limb». In: *IEEE Transactions on Biomedical Engineering* (2008) (cit. on pp. 20, 22, 23).

[41] Arief Z., Sulistijono I. Adji, and Ardiansyah R.A. «Comparison of five time series EMG features extractions using Myo Armband». In: *2015 International Electronics Symposium (IES)*. 2015 (cit. on pp. 20, 22).

[42] Amirabdollahian F. and Walters M.L. «Application of support vector machines in detecting hand grasp gestures using a commercially off the shelf wireless myoelectric armband». In: *IEEE Int Conf Rehabil Robot.* (2017) (cit. on p. 22).

[43] Aramillo-Yánez A., Benalcázar M.E., and Mena-Maldonado E. «Real-Time Hand Gesture Recognition Using Surface Electromyography and Machine Learning: A Systematic Literature Review». In: *Sensors* (2020) (cit. on p. 23).

[44] Ghasemi A. and Zahediasl S. «Normality tests for statistical analysis: a guide for non-statisticians.» In: *Int J Endocrinol Metab* (2012) (cit. on p. 24).

[45] «Statistica non parametrica». In: *Biostatistica in Radiologia: Progettare, realizzare e scrivere un lavoro scientifico radiologico*. Springer Milan, 2008. Chap. 5 (cit. on p. 25).

[46] URL: `https://scikitlearn.org/stable/modules/cross_validation.html` (cit. on p. 27).

[47] D.C. Toledo-Pérez, J. Rodríguez-Reséndiz, and J.C. Gómez-Loenzo R.A.and Jauregui-Correa. «Support Vector Machine-Based EMG Signal Classification Techniques: A Review.» In: *Applied Science* (2019) (cit. on p. 27).

[48] Adilbek Turgunov, Kudratjon Zohirov, Alisher Ganiyev, and Barno Sharopova. «Defining the Features of EMG Signals on the Forearm of the Hand Using SVM, RF, k-NN Classification Algorithms». In: *2020 Information Communication Technologies Conference (ICTC)*. 2020 (cit. on p. 27).

[49] Abdulhamit Subasi. «Classification of EMG signals using PSO optimized SVM for diagnosis of neuromuscular disorders». In: *Computers in Biology and Medicine* 43 (2013) (cit. on pp. 27, 28).

[50] Oskoei M.A. and Hu H. «Support Vector Machine-Based Classification Scheme for Myoelectric Control Applied to Upper Limb». In: *IEEE Transactions on Biomedical Engineering* 55 (2008) (cit. on p. 28).

[51] Chih-Wei H., Chih-Chung C., and Chih-Jen L. «A Practical Guide to Support Vector Classification». In: 2009. URL: `http://www.csie.ntu.edu.tw/~cjlin` (cit. on p. 28).

[52] Silvaggi Nicola. «La forza muscolare». In: *Appunti del corso Scienze motorie (L22), Università degli Studi di Napoli Parthenope* () (cit. on p. 36).